



Published in final edited form as:

*Glia*. 2014 September ; 62(9): 1435–1451. doi:10.1002/glia.22691.

## Activation of the TRPV1 Cation Channel Contributes to Stress-Induced Astrocyte Migration

Karen W. Ho<sup>1</sup>, Wendi S. Lambert<sup>2</sup>, and David J. Calkins<sup>2,3,\*</sup>

<sup>1</sup>Vanderbilt Department of Pharmacology, Vanderbilt University Medical Center, 11425 Medical Research Building IV, Nashville, TN 37232-0654, USA

<sup>2</sup>Vanderbilt Eye Institute, Vanderbilt University Medical Center, 11425 Medical Research Building IV, Nashville, TN 37232-0654, USA

<sup>3</sup>Vanderbilt Brain Institute, Vanderbilt University Medical Center, 11425 Medical Research Building IV, Nashville, TN 37232-0654, USA

### Abstract

Astrocytes provide metabolic, structural and synaptic support to neurons in normal physiology and also contribute widely to pathogenic processes in response to stress or injury. Reactive astrocytes can undergo cytoskeletal reorganization and increase migration through changes in intracellular Ca<sup>2+</sup> mediated by a variety of potential modulators. Here we tested whether migration of isolated retinal astrocytes following mechanical injury (scratch wound) involves the transient receptor potential vanilloid-1 channel (TRPV1), which contributes to Ca<sup>2+</sup>-mediated cytoskeletal rearrangement and migration in other systems. Application of the TRPV1-specific antagonists, capsaizepine (CPZ) or 5<sup>i</sup>-iodoresiniferatoxin (IRTX), slowed migration by as much as 44%, depending on concentration. In contrast, treatment with the TRPV1-specific agonists, capsaicin (CAP) or resiniferatoxin (RTX) produced only a slight acceleration over a range of concentrations. Chelation of extracellular Ca<sup>2+</sup> with EGTA (1 mM) slowed astrocyte migration by 35%. Ratiometric imaging indicated that scratch wound induced a sharp 20% rise in astrocyte Ca<sup>2+</sup> that dissipated with distance from the wound. Treatment with IRTX both slowed and dramatically reduced the scratch-induced Ca<sup>2+</sup> increase. Both CPZ and IRTX influenced astrocyte cytoskeletal organization, especially near the wound edge. Taken together, our results indicate that astrocyte mobilization in response to mechanical stress involves influx of extracellular Ca<sup>2+</sup> and cytoskeletal changes in part mediated by TRPV1 activation.

### Keywords

astrocytes; migration; calcium; TRPV1; reactivity

## INTRODUCTION

Astrocytes distribute widely across the central nervous system (CNS) and provide both metabolic and structural support to neurons as part of normal physiology (Giaume et al. 2010). Astrocytes can also modulate synaptic transmission between neurons through neurotransmitter recycling and the release of gliotransmitters such as glutamate and ATP (Hamilton and Attwell 2010; Wang et al. 2012). In response to neuronal stress or injury, astrocytes undergo reactive hypertrophy of the cell soma and processes (Sofroniew 2009). These morphological changes are associated with an upregulation and redistribution of cytoskeletal proteins, including glial fibrillary acidic protein (GFAP) and actin. Along with changes in morphology, reactive astrocytes undergo a series of functional changes, including increased migration. Remodeling of the actin cytoskeleton plays a major role in migration, involving lamellopodial and filopodial formation and providing the contractile forces needed for movement (Gagelin et al. 1995; Le Clainche and Carrier 2008). Induction of cell protrusions, actin upregulation and polymerization, and upregulation of  $\alpha$ -actinin, an actin-binding protein, all occur in reactive astrocytes in response to disease or injury (Abd-El-Basset and Fedoroff 1997; Moreels et al. 2008; Zhu et al. 2009). Furthermore, astrocytes derived from GFAP/vimentin double-knockout mice have reduced motility, altered cell morphology and reduced capacity for scar formation (Lepekhn et al. 2001; Pekny et al. 1999).

A key regulator of cytoskeletal reorganization and cell motility is  $\text{Ca}^{2+}$ , which mediates downstream signaling cascades that contribute to actin remodeling, retraction of the trailing edge and turnover of adhesion molecules (Wei et al. 2012). Multiple actin-binding proteins that mediate actin crosslinking, capping and severing contain  $\text{Ca}^{2+}$ -binding sites (Glenney et al. 1987; Jayadev et al. 2012). Calcium can also activate other proteins, including calpains, calmodulin, CaMKII and PKC to regulate migration via focal adhesion turnover and cytoskeletal remodeling (Bouvard and Block 1998; Holinstat et al. 2003; Lawson and Maxfield 1995). Astrocytes express a number of potent  $\text{Ca}^{2+}$  modulators, including the transient receptor potential vanilloid-1 channel or TRPV1 (Chen et al. 2009; Doly et al. 2004; Ho et al. 2012; Huang et al. 2010; Mannari et al. 2013). By modulating  $\text{Ca}^{2+}$  levels, TRPV1 activation can lead to cytoskeletal rearrangement including disassembly of microtubules and reorganization of F-actin to drive changes in cell migration (Goswami et al. 2007; Han et al. 2007; Martin et al. 2012). Capsaicin, a TRPV1-specific agonist, increases migration in smooth muscle cells, corneal epithelial cells and hepatoblastoma cells treated with hepatocyte growth factor (Martin et al. 2012; Waning et al. 2007; Yang et al. 2010). In addition to TRPV1, other members of the TRP family, including TRPC and TRPM, can also influence cell motility and migration (Damann et al. 2009; Wei et al. 2009; Zhao et al. 2012).

Astrocytes in the retina envelop and support the axons of retinal ganglion cells and are a critical component of the blood-retinal barrier (Argaw et al. 2012; Scott et al. 2010). As in other brain regions, retinal astrocytes undergo migration and cytoskeletal reorganization in response to both developmental cues (Sakimoto et al. 2012; Watson et al. 2012; Zhang et al. 1999) and disease-related stressors (Agapova et al. 2001; Lin et al. 2012; Tezel et al. 2001). Astrocyte reactivity has been observed in injuries such as retinal detachment, diabetic

retinopathy and glaucoma (DeNiro et al. 2011; Inman and Horner 2007; Luna et al. 2010). Since retinal astrocytes also express TRPV1 (Leonelli et al. 2009), we asked whether the channel could play a role in mediating astrocyte migration in response to mechanical stress. We induced migration of isolated retinal astrocytes using a scratch wound assay and tested how modulation of TRPV1 activation with subunit-specific antagonists (iodo-resiniferatoxin and capsazepine) and agonists (capsaicin and resiniferatoxin) affected the rate of migration. Our results indicate that antagonism of TRPV1 reduces the rate of astrocyte migration through a reduction in  $\text{Ca}^{2+}$  influx and in cytoskeletal remodeling.

## MATERIALS AND METHODS

### Animals

Animal procedures were approved by the Vanderbilt University Medical Center Institutional Animal Care and Use Committee. C57BL/6 (C57) mice were obtained from Jackson Laboratories (Bar Harbor, ME), and Sprague-Dawley rats from Charles River (Wilmington, MA). Animals were maintained in a 12 h light/dark cycle with standard rodent chow available *ad libitum* as described (Crish et al. 2010; Sappington et al. 2010).

### Isolation of primary astrocytes

Primary astrocytes were isolated with immunomagnetic separation as previously described (Sappington et al. 2006). Retinas from post-natal day 1–3 Sprague-Dawley rats were harvested and dissociated with 1 mg/mL papain and mechanical trituration. Astrocytes were isolated with a mouse anti-astrocyte antibody (Leinco Technologies, St. Louis, MO, 4  $\mu\text{g}/\text{mL}$ ) followed by incubation with anti-mouse IgM microbeads (Miltenyi Biotec, Auburn, CA). Cell suspensions were loaded onto pre-equilibrated magnetic columns (Miltenyi Biotec) and allowed to flow through. Isolated cells were seeded onto poly-D-lysine-coated (Sigma-Aldrich, 0.01 mg/mL) T25 flasks and grown until confluent in astrocyte media [DMEM/F12 (Mediatech, Inc. Manassas, VA), 1X G5 supplement (Life Technologies) and 0.1% gentamicin (Life Technologies) plus 10% FBS (Mediatech)].

### Scratch-wound assay

Cover glass chambers (ThermoScientific, Rochester, NY) were coated with 0.01 mg/mL poly-D-lysine. Confluent primary astrocytes were passaged and seeded onto chambers. Once confluent, astrocytes were serum-starved in 0.5% FBS overnight. A single scratch with a 1 mL pipet tip was made through the astrocyte monolayer, and cells were washed three times with serum-free media to remove debris. Cultures were then incubated in astrocyte media plus 0.5% FBS in addition to pharmacological agents. The following TRPV1-specific antagonists were applied 15 min prior to scratch: capsazepine (CPZ; Tocris Bioscience, Bristol, UK, 1  $\mu\text{M}$ –10  $\mu\text{M}$  in ethanol) and 5'-iodo resiniferatoxin (IRTX; Tocris, 300 nM–3  $\mu\text{M}$  in ethanol). The following TRPV1-specific agonists were applied at time 0 h (immediately following the scratch): capsaicin (Sigma-Aldrich, 100 pM–10  $\mu\text{M}$  in ethanol) and resiniferatoxin (RTX; Thermo Fisher Scientific, NJ, 100 pM–10  $\mu\text{M}$  in ethanol). The following chelators were used: ethylene glycol-*bis* (2-aminoethylether)-*N,N,N',N'*-tetraacetic acid (EGTA, Sigma, 100  $\mu\text{M}$ –1 mM in water) and BAPTA-AM (Life Technologies, 1  $\mu\text{M}$ –10  $\mu\text{M}$  in dimethyl sulfoxide). Differential interference contrast (DIC) images were

taken on an inverted Nikon Eclipse Ti microscope at 6 to 12 h intervals post-scratch. A minimum of five images/well were taken, and each treatment was performed in triplicate. Images were taken until the wound for one or more treatments reached 70–100% closure.

### Quantification of astrocyte migration

DIC images for a given treatment were analyzed in blinded fashion to determine the area of the wound at each time point. Briefly, a rectangle was drawn over the cell-free area of the image, which was defined as the area that was minimally 95% free of astrocyte processes. Area was quantified using ImageJ software (Schneider et al. 2012). Preparations with initial wound areas that did not fall within the standard deviation of vehicle were excluded from analysis, leaving 10 to 15 independent images per time point for analysis. The cell-free area at each time point was graphed and linear regression performed to determine the best-fitting line. The slope of each line and its associated error was considered the rate of migration; these were compared between treatments using GraphPad Prism (GraphPad Software, Inc., La Jolla, CA). For each treatment, we also calculated average cell-free area  $\pm$  standard error of the mean (SEM) versus time post-scratch, which is graphed along with the best-fitting regression line.

### Immunohistochemistry

For intact retina, rats and mice were deeply anesthetized with an overdose of sodium pentobarbitol (200 mg/kg, Henry Schein, Inc., Indianapolis, IN) and perfused intracardially with phosphate buffered saline (PBS) followed by 4% paraformaldehyde in PBS. Eyes were enucleated and the retinas harvested. Whole mounted retinas were immunolabeled as previously described. (Crish et al. 2010; Sappington et al. 2010). Retinas were blocked with 10% normal serum and then placed in primary antibody for up to 4 days at 4°C. The following antibodies were used: anti-TRPV1 (for rat, Novus Biologicals, Littleton, CO, 1:1000; for mouse, Neuromics, Edina, MN, 1:100), anti-phosphoneurofilament (pNF; SMI-31, Sternberger Monoclonal, Baltimore, MD, 1:1000) and anti-gial fibrillary acidic protein (GFAP; EMD Millipore, Billerica, MA, 1:500). Immunoreactivity was visualized using appropriate DyLight-conjugated secondary antibodies (Jackson ImmunoResearch, West Grove, PA 1:200). Confocal images were captured using an Olympus FV-1000 inverted microscope.

Naïve astrocyte cultures were fixed in 4% paraformaldehyde. Following scratch-wound assay, cells were fixed in extraction buffer (1 mM EGTA, 1 mM MgCl<sub>2</sub>, 80 mM PIPES, 0.1% saponin, 3% paraformaldehyde) for 20 min at room temperature (Collin et al. 2008). Microtubules were visualized using anti- $\alpha$ -tubulin (Sigma-Aldrich, St. Louis, MO, 1:500; (Sorci et al. 1998) and the appropriate DyLight-conjugated secondary antibodies (Jackson ImmunoResearch, West Grove, PA 1:150). Filamentous actin (F-actin) cytoskeletal microfilaments were labeled with Alexa Fluor 488-phalloidin (Life Technologies, Grand Island, NY, 1:150) in phosphate-buffered saline with 1% bovine serum albumin (Lau et al. 2011). Staining with 4',6-diamidino-2-phenylindole (DAPI; Life Technologies, 1:100) was also performed to visualize nuclei. Confocal images were taken as described above and settings were kept constant for all treatments so that comparisons in label intensity could be

made. Measurements of cell size and intensity were done using ImageJ (Schneider et al. 2012).

### Calcium imaging

Intracellular  $\text{Ca}^{2+}$  was monitored with the fluorescent indicator, fura-2 AM (Molecular Probes, Eugene, OR). Astrocyte cultures were loaded with 5  $\mu\text{M}$  fura-2 AM for 30 minutes at 37°C, rinsed and incubated in DMEM/F12 minus phenol-red with the appropriate pharmacological reagents. Cultures were excited at 340 and 380 nm, and emission collected at 510 nm at 3 second intervals using a Nikon Eclipse Ti inverted microscope with a Roper Scientific black and white camera (Photometrics, Tucson, AZ). After a baseline recording (~30 seconds), a 10  $\mu\text{L}$  pipet tip was used to make a scratch through the astrocyte monolayer. Each treatment had at least 8 replicates. Images were analyzed using NIS Elements software (Nikon, Melville, NY). Regions of interest were drawn at 50, 100, 200 and 400  $\mu\text{m}$  from the edge of the scratch injury (6 regions per distance), and the 340/380 fluorescence ratio was determined over time for each region. Ratios acquired during the scratch and 5 seconds prior to and after injury were excluded due to artifacts. Time-to-peak measurements were determined based on the time after injury required to reach maximum ratios for each treatment.

### Western blot

Confluent astrocytes were serum starved in 0.5% FBS and then pre-incubated for 15 minutes with antagonists prior to scratch. Four parallel wounds with 200  $\mu\text{L}$  pipet tips were made through the astrocyte culture. Cells were washed and incubated with 5  $\mu\text{M}$  CPZ in astrocyte media with 0.5% FBS. Protein lysates were collected in RIPA buffer [50 mM Tris-HCl, 150 mM NaCl, 5 mM EDTA, 0.2 mM sodium vanadate, 1% NP-40, 0.1% SDS, 0.5% sodium deoxycholate, 1 mM phenylmethylsulfonyl fluoride, protease inhibitor cocktail (Roche)]. Protein concentration was determined with the BCA protein assay kit (Pierce). Samples (40 $\mu\text{g}$ ) were separated by SDS-PAGE in 4% to 20% gradient Tris-glycine precast gel (Bio-Rad) following the Western blot protocol from Li-Cor Inc. The following primary antibodies were used: TRPV1 (Novus, 1:2000), GFAP (Millipore, 1:5000), GAPDH (Cell Signaling, 1:1000), actin (Sigma, 1:2000),  $\alpha$ -tubulin (Sigma, 1:2000), tenascin C (Cell Signaling, 1:1000), Cdc42 (Santa Cruz, 1:500), vinculin (Sigma, 1:2000). Proteins were detected using IRDye 680 or IRDye 800CW secondary antibodies, Odyssey Blocking Buffer and a Li-Cor Odyssey Infrared Imaging System (Li-Cor Inc., Lincoln, NE) following manufacturer's protocol.

### Statistical analysis

Data for scratch wound and  $\text{Ca}^{2+}$  analysis is presented as mean  $\pm$  standard error of the mean (SEM) for each treatment. Statistical analysis and p-values for comparing mean cell-free areas were obtained using ANOVA or t-tests for data meeting criteria for normalcy or using non-parametric rank statistics for data failing normalcy using SigmaPlot 11.0 for Windows (Systat Software Inc., Chicago, IL) or GraphPad Prism (GraphPad Software, Inc., La Jolla, CA).

## RESULTS

### Antagonism of TRPV1 Reduces Retinal Astrocyte Migration

Consistent with previous studies (Leonelli et al. 2009), TRPV1 localized to astrocyte cell bodies and processes in both mouse (Figure 1A and 1B) and rat (Figure 1C) retina, as well as to retinal ganglion cells labeled with phospho-neurofilament (Figure 1A and 1C). Higher magnification images and orthogonal views show discrete pockets of colocalization of GFAP and TRPV1 in astrocyte cell bodies and processes (Figure 1B). We observed a similar pattern of TRPV1 expression in cultured astrocytes isolated from rat retina (Figure 2A and 2B). Western blot analysis confirms TRPV1 and GFAP expression in our cultured astrocytes (Figure 2C). We detected four TRPV1 isoforms in our astrocytes, similar to those found in neuroblastoma cells (Lilja et al. 2007), with the doublet below 75 kDa having been specifically reported in astrocytes (Huang et al. 2010; Lilja et al. 2007).

We treated isolated astrocytes with the TRPV1-specific antagonists capsaizepine (CPZ) or 5'-iodoresiniferatoxin (IRTX; (Seabrook et al. 2002; Wahl et al. 2001; Walpole et al. 1994) prior to scratch to discern whether blocking activation would influence migration. Figure 3 shows representative images of CPZ-treated astrocytes following scratch. In the vehicle group, the initial cell-free area was reduced at 36 h by astrocytes migrating from the edges (Figure 3A). Treatment with 1  $\mu\text{M}$  CPZ had little effect on wound closure compared to vehicle (Figure 3B). However, treatment with 10  $\mu\text{M}$  CPZ reduced wound closure, resulting in a considerably larger cell-free area at 36 h compared to vehicle or 1  $\mu\text{M}$  CPZ (Figure 3C). Similar results were obtained with 5  $\mu\text{M}$  CPZ and 3  $\mu\text{M}$  IRTX (not shown). Antagonists did not affect cell morphology compared to vehicle.

When quantified, the deceleration with CPZ was significant (Figure 4A). For the vehicle group, an initial wound area of  $9.4 \pm 0.1 \mu\text{m}^2 (\times 10^5)$  was reduced 75% at 36 h following injury. While treatment with 1  $\mu\text{M}$  CPZ resulted in similar closure at 36 h (77%,  $p = 0.65$ ), both 5 and 10  $\mu\text{M}$  CPZ significantly reduced closure to 44% ( $p = 0.001$ ) and 38% ( $p = 0.001$ ), respectively. Accordingly, the rate of astrocyte migration – defined as the slope of the best-fit linear regression – also differed with increasing CPZ (Figure 4B). Compared to vehicle ( $1.00 \pm 0.03 \mu\text{m}^2/\text{h}$ ), 5 and 10  $\mu\text{M}$  CPZ reduced migration rate by 41% ( $0.59 \pm 0.06 \mu\text{m}^2/\text{h}$ ) and 44% ( $0.56 \pm 0.06 \mu\text{m}^2/\text{h}$ ), respectively ( $p = 0.006$ ). The 15% reduction with 1  $\mu\text{M}$  CPZ ( $0.85 \pm 0.04 \mu\text{m}^2/\text{h}$ ) was not significant ( $p = 0.064$ ). Migration was also decelerated by a second TRPV1 antagonist, IRTX (Figure 4C). Vehicle-treated cells with an initial wound area of  $12.54 \pm 0.31 \mu\text{m}^2 (\times 10^5)$  showed a closure of 76% at 36 h after injury. Treatment with 300 nM or 1  $\mu\text{M}$  IRTX had no effect compared to vehicle (67% and 75% respectively,  $p > 0.08$ ), while 3  $\mu\text{M}$  IRTX reduced closure to 52% of initial wound ( $p = 0.001$ ). Similarly, while 300 nM and 1  $\mu\text{M}$  IRTX had little effect on rate compared to vehicle (Figure 4D;  $p = 0.687$ ), 3  $\mu\text{M}$  IRTX reduced the rate by 28% ( $0.72 \pm 0.07 \mu\text{m}^2/\text{h}$ ;  $p = 0.035$ ).

### TRPV1 Agonism has Modest Effects on Astrocyte Migration

Next we treated astrocytes immediately following scratch with the specific agonists capsaicin (CAP) or resiniferatoxin (RTX; (Caterina et al. 2000; Caterina et al. 1997;

Raisinghani et al. 2005; Szallasi and Blumberg 1989), which had no effect on cell morphology (data not shown). Compared with the TRPV1 antagonists, the initial wounds in the agonist experiments were 31% smaller (Figure 5A). Accordingly, closure occurred earlier. At 24 h post-injury, treatment with 100 nM and 1  $\mu$ M CAP induced closure of 74% and 64%, respectively, compared to 62% with vehicle (Figure 5A). This difference was not significant ( $p = 0.231$ ), nor was the 46% closure observed with 10  $\mu$ M CAP ( $p = 0.098$ ). A range of concentrations from 100 pM to 1  $\mu$ M CAP showed accelerations of 8–23% ( $p = 0.26$ ; Figure 5B). The exception was the highest concentration (10  $\mu$ M), which decelerated migration by 9% ( $p = 0.66$ ). For the second agonist RTX (Figure 5C), treatment with 100 pM or 1 nM induced closure of 59% and 52%, similar to the 52% closure with vehicle ( $p = 0.289$ ). As with CAP, the highest concentration of RTX (10  $\mu$ M) reduced closure to 38% at 24 h ( $p = 0.056$ ). When comparing migration rates (Figure 5D), treatment with 100 pM or 1  $\mu$ M RTX accelerated migration 26% and 11%, respectively ( $p = 0.268$ ). A near 30% reduction in rate with 10  $\mu$ M RTX was not significant ( $p = 0.186$ ).

### Chelation of Extracellular but not Intracellular $\text{Ca}^{2+}$ Reduces Astrocyte Migration

Since  $\text{Ca}^{2+}$  is a key regulator of cytoskeletal reorganization and cell motility (Wei et al. 2012), we used EGTA or BAPTA-AM to examine the role of extracellular or intracellular  $\text{Ca}^{2+}$ , respectively, in astrocyte migration (Figure 6). Neither EGTA nor BAPTA-AM affected astrocyte morphology at the concentrations used (data not shown). We found that 1 mM EGTA led to only 40% closure after 48 h, compared to 65% for vehicle (Figure 6A). Although the percent wound closure did not differ ( $p = 0.052$ ), the migration rate for 1 mM EGTA was 45% slower compared to vehicle (Figure 6B;  $p = 0.048$ ). The modest increase in rate with 100  $\mu$ M EGTA (9%) was not significant ( $p = 0.48$ ). In contrast, chelation of intracellular  $\text{Ca}^{2+}$  with 1  $\mu$ M or 10  $\mu$ M BAPTA-AM had little effect, with 65% and 70% closure, respectively, at 36 h compared to 73% for vehicle (Figure 6C;  $p = 0.106$ ). Migration rate following BAPTA-AM treatment was also similar ( $p = 0.53$ ; Figure 6D).

### Antagonism of TRPV1 Reduces and Slows Calcium Influx Following Injury

Astrocyte cultures loaded with the  $\text{Ca}^{2+}$  indicator fura-2 AM followed by ratiometric imaging show little variation in basal levels (Figure 7A). At 10 s following scratch, intracellular  $\text{Ca}^{2+}$  increased especially near the leading edge (Figure 7B). Pre-treatment with the TRPV1-specific antagonists CPZ (10  $\mu$ M; Figure 7C) and IRTX (3  $\mu$ M; Figure 7D) appeared to reduce this increase. We quantified the 340/380 nm  $\text{Ca}^{2+}$  ratio over time at discrete distances from the scratch-wound edge (50, 100, 200 and 400  $\mu$ m), both with and without the antagonists (Figure 8). Following scratch injury, vehicle astrocytes demonstrated a sharp rise in  $\text{Ca}^{2+}$  that diminished both over time and with increasing distance from the leading edge. At 50  $\mu$ m, this increase was almost 20%, compared to about 4% at 400  $\mu$ m. Treatment with 10  $\mu$ M CPZ seemed to have little effect on  $\text{Ca}^{2+}$  influx, except to slow the time to peak. In contrast, 3  $\mu$ M IRTX dramatically reduced the increase in intracellular  $\text{Ca}^{2+}$  following injury to 8% at 50  $\mu$ m from the wound. IRTX also seemed to slow the time to peak  $\text{Ca}^{2+}$  following scratch. The magnitudes of these changes were reduced at 100, 200 and 400  $\mu$ m from the injury edge, although the trends remain the same.

Quantification of the data in Figure 8 shows that neither 10  $\mu\text{M}$  CPZ nor 3  $\mu\text{M}$  IRTX significantly influenced basal (i.e., pre-wound) levels of  $\text{Ca}^{2+}$  compared to vehicle (Figure 9A). However, antagonists did slow the time to peak  $\text{Ca}^{2+}$  following scratch (Figure 9B). Compared to vehicle, 3  $\mu\text{M}$  IRTX slowed the time to peak by over three-fold at 50, 100 and 200  $\mu\text{m}$  from the scratch ( $p = 0.007$ ). Treatment with 10  $\mu\text{M}$  CPZ also slowed the time to peak at 100  $\mu\text{m}$  from the wound ( $p = 0.025$ ). At 400  $\mu\text{m}$ , the times to peak for the antagonists did not differ significantly from vehicle. Similarly, treatment with 3  $\mu\text{M}$  IRTX induced the greatest difference between basal and post-scratch  $\text{Ca}^{2+}$  compared to vehicle across distances from the wound (Figure 9C). In the interval 5–30 s following scratch, IRTX reduced the change in  $\text{Ca}^{2+}$  ratio by 55–80% at all distances from the injury ( $p = 0.04$ ). IRTX also reduced the change in  $\text{Ca}^{2+}$  from basal at subsequent intervals following injury, although the reductions were not significant ( $p = 0.062$ ). Treatment with CPZ, while generally slowing the time to peak (Figure 9B), had little effect on the magnitude of the change in  $\text{Ca}^{2+}$  following scratch ( $p = 0.39$ ).

### Antagonism of TRPV1 Reduces Cell Area and Modifies Cytoskeletal Components

We speculated that TRPV1 may also play a role in the expression and localization of cytoskeletal components after injury. We collected protein from naïve astrocytes and astrocytes 12 h after scratch and performed Western blots for cytoskeletal and migration-related proteins (Figure 10). We chose this time based on wound closure progression with antagonists (Figure 4) and on literature showing peak expression of GFAP and tenascin C secretion at this time following scratch injury (Gao et al. 2013; Nishio et al. 2005). Vehicle treatment following scratch slightly increased expression of the cytoskeletal components,  $\alpha$ -tubulin, actin and GFAP, about 5–13% compared to unscratched naïve astrocytes ( $p = 0.147$ ). Similarly, the expression of proteins involved in focal adhesion and migration — tenascin C, Cdc42 and vinculin (Abd-el-Basset et al. 1991; Etienne-Manneville and Hall 2001; Nishio et al. 2005) — slightly increased 10–20% following scratch ( $p = 0.206$ ). Treatment with 5  $\mu\text{M}$  CPZ reduced expression of cytoskeletal and migration-related proteins 3–18% compared to vehicle ( $p = 0.224$ ), with the exception of GFAP which remained slightly elevated.

Next, we examined the localization of  $\alpha$ -tubulin and F-actin in astrocytes at the leading edge of the wound (Figure 11). At 36 h post-scratch,  $\alpha$ -tubulin in vehicle-treated cells concentrated in the perinuclear region, with microtubules extending into astrocyte processes (Figure 11A and 11B, red). F-actin microfilaments distributed throughout the cytoplasm in parallel arrays that also extended into processes (Figure 11A and 11B, green). We observed very little colocalization between  $\alpha$ -tubulin and F-actin. Treatment with 10  $\mu\text{M}$  CPZ appeared to reduce astrocyte size, though the pattern of F-actin and  $\alpha$ -tubulin labeling was similar to vehicle (Figure 11A). Astrocytes treated with 3  $\mu\text{M}$  IRTX did not appear to contract (Figure 11B), but both F-actin and  $\alpha$ -tubulin appeared more intense with more extensive co-localization. When quantified (Figure 11C), 5 and 10  $\mu\text{M}$  CPZ reduced astrocyte cytoplasmic area by 42% and 29%, respectively ( $p = 0.003$ ). Although 3  $\mu\text{M}$  IRTX also reduced cell area (12%), this was not significant ( $p = 0.20$ ). Similarly, levels of  $\alpha$ -tubulin were reduced by 17% with 10  $\mu\text{M}$  CPZ ( $p = 0.006$ , Figure 11D), while IRTX had

little effect ( $p = 0.078$ ). In contrast, F-actin intensities were similar for CPZ compared to vehicle ( $p = 0.11$ ), but increased 26% for 3  $\mu\text{M}$  IRTX (Figure 11D;  $p < 0.0001$ ).

To better understand changes in the subcellular localization of cytoskeletal proteins during injury-induced migration, we captured high magnification images of  $\alpha$ -tubulin and F-actin in astrocytes at the leading edge of the scratch wound. Astrocytes treated with vehicle and immunolabeled for  $\alpha$ -tubulin show clearly defined microtubules that radiate from the microtubule organizing center near the nucleus and extend into processes at the leading edge (Figure 12A). Localization is most intense near the leading edge (Figure 12B). This rearrangement of the microtubule organizing center establishes cell polarity and directs migration toward the cell-free area (Etienne-Manneville and Hall 2001). In cells treated with 5  $\mu\text{M}$  CPZ, microtubules appear less intense and retracted within individual processes (Figure 12A). Closer to the edge of individual processes (Figure 12B; dotted line), microtubules appear less defined and take on a fragmented appearance that is exacerbated with 10  $\mu\text{M}$  CPZ. Astrocytes treated with 3  $\mu\text{M}$  IRTX had clearly defined microtubules extending from the microtubule organizing center into processes that appeared less intense near the edge compared to vehicle-treated cells. Labeling for F-actin in vehicle-treated astrocytes shows intense localization at filopodia extending toward the leading edge and cell periphery (Figure 12C and D). This reorganization of actin filaments provides the contractile force necessary to drive cell migration (Le Clairche and Carrier, 2008). Actin intensity was reduced in astrocytes treated with CPZ, as was its localization to filopodia (Figure 12D; dotted line). This effect was more pronounced with 10  $\mu\text{M}$  CPZ. In cells treated with IRTX, F-actin intensity appeared similar to vehicle, but localization was less near the cell edge. These results indicate that with injury, TRPV1 activation is associated with moderate cytoskeletal remodeling in astrocytes at the leading edge.

## DISCUSSION

We have shown that TRPV1 expressed in retinal astrocytes (Figures 1 and 2) contributes to migration in response to mechanical injury. Using a scratch wound assay, we demonstrated that pre-treatment with the TRPV1-specific antagonists capsazepine (CPZ) or 5'-iodoresiniferatoxin (IRTX) slowed migration of retinal astrocytes maintained in culture by as much as 44%, depending on concentration (Figures 3 and 4). In contrast, treatment with the TRPV1-specific agonists, capsaicin (CAP) or resiniferatoxin (RTX) had minimal effect on astrocyte mobility (Figure 5). Furthermore, astrocyte migration in the scratch wound assay is at least partly dependent upon an increase in intracellular  $\text{Ca}^{2+}$ , primarily from extracellular influx, as chelation with EGTA, but not BAPTA-AM also slowed migration (Figure 6). The increase in astrocyte intracellular  $\text{Ca}^{2+}$  in response to scratch injury was mediated in part by TRPV1, since ratiometric imaging revealed that IRTX could both slow this change and lower its magnitude (Figures 7–9). Finally, it appears TRPV1 also contributes to astrocyte migration through rearrangement of the cytoskeleton, as TRPV1 antagonist CPZ reduced  $\alpha$ -tubulin intensity, decreased cell size, and caused retraction and fragmentation of microfilaments in astrocytes after scratch wound (Figures 10–12).

Based upon our results, we propose a mechanism for TRPV1 modulation of injury-induced migration in astrocytes (Figure 13). Under basal conditions, retinal astrocytes expressing

TRPV1 maintain focal adhesions with the extracellular matrix via cytoskeletal elements, such as actin stress fibers and microtubules (Etienne-Manneville and Hall, 2001; Le Clainche and Carlier, 2008). Following mechanical injury, activated TRPV1 increases  $\text{Ca}^{2+}$  levels within astrocytes nearest the injury. The influx of extracellular  $\text{Ca}^{2+}$  likely activates signaling pathways that alter the subcellular localization of cytoskeletal proteins. Establishment of cell polarity by microtubule rearrangement and localization of actin to filopodia at the leading edge facilitates migration of astrocytes into the wound area. Treatment with TRPV1 antagonists slows astrocyte migration by decreasing  $\text{Ca}^{2+}$  influx and/or cytoskeletal remodeling.

TRPV1 is expressed broadly in neurons of both the peripheral and central nervous systems (Leonelli et al. 2009; Toth et al. 2005a). In the retina, TRPV1 is expressed in multiple neuronal and glial cell types, including photoreceptors, retinal ganglion cells, microglia and astrocytes (Sappington and Calkins 2008; Sappington et al. 2009; Zimov and Yazulla 2004). In glia, TRPV1 contributes to Muller cell reactivity following axotomy, and to  $\text{Ca}^{2+}$ -dependent release of IL-6 in microglia under increased hydrostatic pressure (Leonelli et al. 2010; Sappington and Calkins 2008). Astrocytic TRPV1 contributes to pH-related responses and increased expression of intermediate filaments after injury (Chen et al. 2009; Huang et al. 2010). As a  $\text{Ca}^{2+}$  channel, TRPV1 localizes primarily to the plasma membrane in punctate pockets (Leonelli et al. 2009; Saunders et al. 2007). However, diffuse TRPV1 immunolabeling, similar to what we observed in retinal astrocytes (Figures 1 and 2), also occurs in astrocytes of the substantia nigra (Marinelli et al. 2007).

Several groups have shown that TRPV1 contributes to cell migration. In hepatoblastoma cells, Waning *et al.* showed that although capsaicin alone did not increase cell migration, it did enhance migration in response to hepatocyte growth factor, an effect that was inhibited by CPZ (Waning et al. 2007). Yang *et al.* showed that TRPV1 mediated migration of corneal epithelial cells after scratch wound injury (Yang et al. 2010). While CPZ alone did not affect migration, it did prevent the capsaicin-induced increase in migration (Yang et al. 2010). Similarly, in pulmonary arterial smooth muscle cells, TRPV1 activation increased migration, which was blocked by CPZ (Martin et al. 2012). In our retinal astrocytes, TRPV1 antagonism with CPZ or IRTX reduced wound closure over time (Figures 3 and 4). We found that agonism with either capsaicin or RTX had little effect on migration (Figure 5), suggesting a ceiling effect. Thus, TRPV1 could be activated to such a level by the injury alone that further activation is not possible. This effect could also be mediated by other factors present in the wound milieu. Possible candidates include the endocannabinoids, such as anandamide, which are produced and released by astrocytes and can also influence their migration (Song and Zhong 2000; Walter et al. 2002).

We found that for retinal astrocytes, scratch injury increases intracellular  $\text{Ca}^{2+}$  (Figures 7–9). The increase in  $\text{Ca}^{2+}$  we observed was not unexpected, as another member of the TRP family, TRPM7, becomes activated in response to shear stress and contributes to fibroblast migration (Wei et al. 2009). In our injury model, IRTX significantly reduced the scratch-induced  $\text{Ca}^{2+}$  increase, while CPZ had only modest effects. This could be due to a species-dependent difference in efficacy that has been observed for CPZ, as this antagonist only weakly inhibits  $\text{Ca}^{2+}$  currents in rat TRPV1 compared to human TRPV1 (McIntyre et al.

2001; Phillips et al. 2004). IRTX, however, does not have this selectivity and has far greater efficacy (Correll et al. 2004). Similar differences in  $\text{Ca}^{2+}$  responses have been shown for TRPV1 agonists as well, emphasizing the complexity of TRP vanilloid subunit pharmacology. For example, Toth et al. found qualitative differences in  $\text{Ca}^{2+}$  influx when cells are treated with various TRPV1 agonists (Toth et al. 2005b). In response to capsaicin, cells exhibited an immediate increase in  $\text{Ca}^{2+}$ , but with RTX there was minimal initial increase but a sharp subsequent increase, suggesting a latency in cellular response to RTX. Furthermore, higher concentrations of capsaicin increased the maximal amount of  $\text{Ca}^{2+}$  influx, an effect not seen with RTX treatment. Rather, the number of cells that responded increased with higher RTX concentrations. As CPZ and IRTX are analogs of capsaicin and RTX, respectively, it is possible the qualitative differences in  $\text{Ca}^{2+}$  influx seen with the agonists might be extrapolated to the antagonists (Bevan et al. 1992; Wahl et al. 2001).

In addition to activation by capsaicin and RTX, TRPV1 can also be activated by a variety of other effectors, including pH, heat and endocannabinoids, which can be blocked by both CPZ and IRTX in various systems (Marinelli et al. 2003; Seabrook et al. 2002; Zygmunt et al. 1999). This suggests the presence of multiple binding sites for the antagonists in addition to the vanilloid binding sites. The ability of antagonists to inhibit these stimuli can also vary, as CPZ can block pH activation in guinea pigs but not in rats (McIntyre et al. 2001; Savidge et al. 2002). The environment of TRPV1 can also influence its activation and regulation. For example, TRPV1 contains multiple phosphorylation sites for PKA, PKC and protein phosphatase 2B that sensitize and desensitize the channel (Suh and Oh 2005). Addition of cyclosporin A, an inhibitor for protein phosphatase 2B, increases the potency of TRPV1 agonists 1.1-fold for RTX to as much as 7.8-fold for DA-5018. The potency for capsaicin increased 2.1-fold. Similar to agonists, cyclosporin A increased antagonist potencies from 1.1-fold to 2.5-fold (Pearce et al. 2008). This suggests that the signaling environment and phosphorylation state of TRPV1 have profound effects on the channel's sensitivity to ligands. In the injury milieu, cross-talk between a variety of effectors, receptors, and signaling pathways could modulate the structure and state of TRPV1, potentially affecting the efficacy of TRPV1 pharmacological agents. Together, these differences could explain why CPZ had the greater inhibitory effect on migration, while IRTX had the more robust effect on intracellular  $\text{Ca}^{2+}$  levels.

Activation of TRPV1 leads to an increase in intracellular  $\text{Ca}^{2+}$ , itself an important signaling molecule in migration (Wei et al. 2012). Calcium can regulate downstream signaling cascades that influence migration through cytoskeletal remodeling and focal adhesion turnover (Ridley et al. 2003). Multiple proteins involved in actin remodeling, including  $\alpha$ -actinin and gelsolin, are regulated by  $\text{Ca}^{2+}$  and  $\text{Ca}^{2+}$ -binding proteins like calpains and calmodulin (Gremm and Wegner 2000; Hartwig et al. 1992; Shao et al. 2013). In addition,  $\text{Ca}^{2+}$  also regulates focal adhesions, which link the cytoskeleton to the extracellular matrix. Activation of TRPV1 by capsaicin can lead to cytoskeletal remodeling involving rearrangement of F-actin and tubulin networks (Goswami et al. 2006; Martin et al. 2012). For example, in a submandibular gland cell line, capsaicin induces cytoskeletal rearrangement by decreasing the amount of actin and increasing the space between each filament (Cong et al. 2013). In pulmonary smooth muscle cells and neutrophils, however, capsaicin increased actin levels but had no significant effect on the tubulin cytoskeleton

(Martin et al. 2012; Wang et al. 2005). TRPV1 also localizes to the tips of filopodia and induces filopodia formation and microtubule disassembly in a dorsal root ganglia cell line (Goswami et al. 2006; Goswami and Hucho 2007). We observed that inhibition of TRPV1 following scratch-wound increased F-actin levels but decreased  $\alpha$ -tubulin in migrating astrocytes (Figure 11). Higher magnification images of astrocytes at the leading edge following TRPV1 antagonism showed microtubule fragmentation and retraction from the cell edge (Figure 12) suggesting TRPV1 modulates cytoskeletal rearrangement and subcellular localization after injury.

Cell migration is a key response during stress and injury. Astrocyte migration is one of the functional changes that occur during reactive gliosis and glial scar formation, which can act as a barrier against axon regeneration (Li et al. 2012; Saadoun et al. 2005). Migration involved in scar formation, however, can also be a beneficial response by confining inflammatory cells and compressing the lesion (Renault-Mihara et al. 2008; Sun et al. 2013). Reactive astrocytes have been observed in neurodegenerative diseases such Alzheimer's Disease and glaucoma (Inman and Horner 2007; Liu et al. 2012). Understanding the molecular mechanisms that underlie reactive gliosis and astrocyte migration could lead to potential therapeutic interventions in these and other neurodegenerative diseases.

## Acknowledgments

### ACKNOWLEDGMENTS AND SUPPORT

Funding provided by the National Eye Institute (5R01EY017427-03; DJC), the Melza M. and Frank Theodore Barr Foundation through the Glaucoma Research Foundation (DJC), Senior Scientific Investigator and Departmental Unrestricted Award from Research to Prevent Blindness, Inc. (DJC), a BrightFocus Foundation (formerly American Health Assistance Foundation) National Glaucoma Research Award (DJC), the Vanderbilt Pharmacology Training Grant (T32GM007628-32; KWH). Imaging supported through the Vanderbilt University Medical Center Cell Imaging Shared Resource core facility (CTSA grant UL1 RR024975 from NCRR/NIH) and the Vanderbilt Vision Research Center (P30EY008126).

## BIBLIOGRAPHY

- Abd-el-Basset EM, Ahmed I, Fedoroff S. Actin and actin-binding proteins in differentiating astroglia in tissue culture. *J Neurosci Res.* 1991; 30(1):1–17. [PubMed: 1795393]
- Abd-El-Basset EM, Fedoroff S. Upregulation of F-actin and alpha-actinin in reactive astrocytes. *J Neurosci Res.* 1997; 49(5):608–616. [PubMed: 9302082]
- Agapova OA, Ricard CS, Salvador-Silva M, Hernandez MR. Expression of matrix metalloproteinases and tissue inhibitors of metalloproteinases in human optic nerve head astrocytes. *Glia.* 2001; 33(3): 205–216. [PubMed: 11241738]
- Argaw AT, Asp L, Zhang J, Navrazhina K, Pham T, Mariani JN, Mahase S, Dutta DJ, Seto J, Kramer EG, et al. Astrocyte-derived VEGF-A drives blood-brain barrier disruption in CNS inflammatory disease. *J Clin Invest.* 2012; 122(7):2454–2468. [PubMed: 22653056]
- Bevan S, Hothi S, Hughes G, James IF, Rang HP, Shah K, Walpole CS, Yeats JC. Capsazepine: a competitive antagonist of the sensory neurone excitant capsaicin. *Br J Pharmacol.* 1992; 107(2): 544–552. [PubMed: 1422598]
- Bouvard D, Block MR. Calcium/calmodulin-dependent protein kinase II controls integrin  $\alpha$ 5 $\beta$ 1-mediated cell adhesion through the integrin cytoplasmic domain associated protein-1 $\alpha$ . *Biochem Biophys Res Commun.* 1998; 252(1):46–50. [PubMed: 9813144]
- Caterina MJ, Leffler A, Malmberg AB, Martin WJ, Trafton J, Petersen-Zeitz KR, Koltzenburg M, Basbaum AI, Julius D. Impaired nociception and pain sensation in mice lacking the capsaicin receptor. *Science.* 2000; 288(5464):306–313. [PubMed: 10764638]

- Caterina MJ, Schumacher MA, Tominaga M, Rosen TA, Levine JD, Julius D. The capsaicin receptor: a heat-activated ion channel in the pain pathway. *Nature*. 1997; 389(6653):816–824. [PubMed: 9349813]
- Chen Y, Willcockson HH, Valtschanoff JG. Influence of the vanilloid receptor TRPV1 on the activation of spinal cord glia in mouse models of pain. *Exp Neurol*. 2009; 220(2):383–390. [PubMed: 19815011]
- Collin L, Schlessinger K, Hall A. APC nuclear membrane association and microtubule polarity. *Biol Cell*. 2008; 100(4):243–252. [PubMed: 18042042]
- Cong X, Zhang Y, Yang NY, Li J, Ding C, Ding QW, Su YC, Mei M, Guo XH, Wu LL, et al. Occludin is required for TRPV1-modulated paracellular permeability in the submandibular gland. *J Cell Sci*. 2013; 126(Pt 5):1109–1121. [PubMed: 23345400]
- Correll CC, Phelps PT, Anthes JC, Umland S, Greenfeder S. Cloning and pharmacological characterization of mouse TRPV1. *Neurosci Lett*. 2004; 370(1):55–60. [PubMed: 15489017]
- Crish SD, Sappington RM, Inman DM, Horner PJ, Calkins DJ. Distal axonopathy with structural persistence in glaucomatous neurodegeneration. *Proc Natl Acad Sci U S A*. 2010; 107(11):5196–5201. [PubMed: 20194762]
- Damann N, Owsianik G, Li S, Poll C, Nilius B. The calcium-conducting ion channel transient receptor potential canonical 6 is involved in macrophage inflammatory protein-2-induced migration of mouse neutrophils. *Acta Physiol (Oxf)*. 2009; 195(1):3–11. [PubMed: 18983454]
- DeNiro M, Al-Mohanna FH, Al-Mohanna FA. Inhibition of reactive gliosis prevents neovascular growth in the mouse model of oxygen-induced retinopathy. *PLoS One*. 2011; 6(7):e22244. [PubMed: 21779402]
- Doly S, Fischer J, Salio C, Conrath M. The vanilloid receptor-1 is expressed in rat spinal dorsal horn astrocytes. *Neurosci Lett*. 2004; 357(2):123–126. [PubMed: 15036590]
- Etienne-Manneville S, Hall A. Integrin-mediated activation of Cdc42 controls cell polarity in migrating astrocytes through PKCzeta. *Cell*. 2001; 106(4):489–498. [PubMed: 11525734]
- Gagelin C, Pierre M, Gavaret JM, Toru-Delbauffe D. Rapid TGF beta 1 effects on actin cytoskeleton of astrocytes: comparison with other factors and implications for cell motility. *Glia*. 1995; 13(4):283–293. [PubMed: 7615337]
- Gao K, Wang CR, Jiang F, Wong AY, Su N, Jiang JH, Chai RC, Vatcher G, Teng J, Chen J, et al. Traumatic scratch injury in astrocytes triggers calcium influx to activate the JNK/c-Jun/AP-1 pathway and switch on GFAP expression. *Glia*. 2013; 61(12):2063–2077. [PubMed: 24123203]
- Giaume C, Koulakoff A, Roux L, Holcman D, Rouach N. Astroglial networks: a step further in neuroglial and gliovascular interactions. *Nat Rev Neurosci*. 2010; 11(2):87–99. [PubMed: 20087359]
- Glenney JR Jr, Tack B, Powell MA. Calpactins: two distinct Ca<sup>++</sup>-regulated phospholipid- and actin-binding proteins isolated from lung and placenta. *J Cell Biol*. 1987; 104(3):503–511. [PubMed: 2950118]
- Goswami C, Dreger M, Otto H, Schwappach B, Hucho F. Rapid disassembly of dynamic microtubules upon activation of the capsaicin receptor TRPV1. *J Neurochem*. 2006; 96(1):254–266. [PubMed: 16336230]
- Goswami C, Hucho T. TRPV1 expression-dependent initiation and regulation of filopodia. *J Neurochem*. 2007; 103(4):1319–1333. [PubMed: 17714453]
- Goswami C, Schmidt H, Hucho F. TRPV1 at nerve endings regulates growth cone morphology and movement through cytoskeleton reorganization. *FEBS J*. 2007; 274(3):760–772. [PubMed: 17288556]
- Gremm D, Wegner A. Gelsolin as a calcium-regulated actin filament-capping protein. *Eur J Biochem*. 2000; 267(14):4339–4345. [PubMed: 10880956]
- Hamilton NB, Attwell D. Do astrocytes really exocytose neurotransmitters? *Nat Rev Neurosci*. 2010; 11(4):227–238. [PubMed: 20300101]
- Han P, McDonald HA, Bianchi BR, Kouhen RE, Vos MH, Jarvis MF, Faltynek CR, Moreland RB. Capsaicin causes protein synthesis inhibition and microtubule disassembly through TRPV1 activities both on the plasma membrane and intracellular membranes. *Biochem Pharmacol*. 2007; 73(10):1635–1645. [PubMed: 17274957]

- Hartwig JH, Thelen M, Rosen A, Janmey PA, Nairn AC, Aderem A. MARCKS is an actin filament crosslinking protein regulated by protein kinase C and calcium-calmodulin. *Nature*. 1992; 356(6370):618–622. [PubMed: 1560845]
- Ho KW, Ward NJ, Calkins DJ. TRPV1: a stress response protein in the central nervous system. *Am J Neurodegener Dis*. 2012; 1(1):1–14. [PubMed: 22737633]
- Holinstat M, Mehta D, Kozasa T, Minshall RD, Malik AB. Protein kinase C $\alpha$ -induced p115RhoGEF phosphorylation signals endothelial cytoskeletal rearrangement. *J Biol Chem*. 2003; 278(31):28793–28798. [PubMed: 12754211]
- Huang C, Hu ZL, Wu WN, Yu DF, Xiong QJ, Song JR, Shu Q, Fu H, Wang F, Chen JG. Existence and distinction of acid-evoked currents in rat astrocytes. *Glia*. 2010; 58(12):1415–1424. [PubMed: 20549751]
- Inman DM, Horner PJ. Reactive nonproliferative gliosis predominates in a chronic mouse model of glaucoma. *Glia*. 2007; 55(9):942–953. [PubMed: 17457855]
- Jayadev R, Kuk CY, Low SH, Murata-Hori M. Calcium sensitivity of alpha-actinin is required for equatorial actin assembly during cytokinesis. *Cell Cycle*. 2012; 11(10):1929–1937. [PubMed: 22544326]
- Lau CL, O'Shea RD, Broberg BV, Bischof L, Beart PM. The Rho kinase inhibitor Fasudil up-regulates astrocytic glutamate transport subsequent to actin remodelling in murine cultured astrocytes. *Br J Pharmacol*. 2011; 163(3):533–545. [PubMed: 21309758]
- Lawson MA, Maxfield FR. Ca<sup>2+</sup>- and calcineurin-dependent recycling of an integrin to the front of migrating neutrophils. *Nature*. 1995; 377(6544):75–79. [PubMed: 7544874]
- Le Clainche C, Carlier MF. Regulation of actin assembly associated with protrusion and adhesion in cell migration. *Physiol Rev*. 2008; 88(2):489–513. [PubMed: 18391171]
- Leonelli M, Martins DO, Britto LR. TRPV1 receptors are involved in protein nitration and Muller cell reaction in the acutely axotomized rat retina. *Exp Eye Res*. 2010; 91(5):755–768. [PubMed: 20826152]
- Leonelli M, Martins DO, Kihara AH, Britto LR. Ontogenetic expression of the vanilloid receptors TRPV1 and TRPV2 in the rat retina. *Int J Dev Neurosci*. 2009; 27(7):709–718. [PubMed: 19619635]
- Lepkhin EA, Eliasson C, Berthold CH, Berezin V, Bock E, Pekny M. Intermediate filaments regulate astrocyte motility. *J Neurochem*. 2001; 79(3):617–625. [PubMed: 11701765]
- Li Y, Li D, Ibrahim A, Raisman G. Repair involves all three surfaces of the glial cell. *Prog Brain Res*. 2012; 201:199–218. [PubMed: 23186716]
- Lilja J, Lindgren H, Forsby A. Surfactant-induced TRPV1 activity—a novel mechanism for eye irritation? *Toxicol Sci*. 2007; 99(1):174–180. [PubMed: 17575321]
- Lin CC, Hsieh HL, Shih RH, Chi PL, Cheng SE, Chen JC, Yang CM. NADPH oxidase 2-derived reactive oxygen species signal contributes to bradykinin-induced matrix metalloproteinase-9 expression and cell migration in brain astrocytes. *Cell Commun Signal*. 2012; 10(1):35. [PubMed: 23176293]
- Liu XP, Zheng HY, Qu M, Zhang Y, Cao FY, Wang Q, Ke D, Liu GP, Wang JZ. Upregulation of astrocytes protein phosphatase-2A stimulates astrocytes migration via inhibiting p38 MAPK in tg2576 mice. *Glia*. 2012; 60(9):1279–1288. [PubMed: 22729898]
- Luna G, Lewis GP, Banna CD, Skalli O, Fisher SK. Expression profiles of nestin and synemin in reactive astrocytes and Muller cells following retinal injury: a comparison with glial fibrillar acidic protein and vimentin. *Mol Vis*. 2010; 16:2511–2523. [PubMed: 21139996]
- Mannari T, Morita S, Furube E, Tominaga M, Miyata S. Astrocytic TRPV1 ion channels detect blood-borne signals in the sensory circumventricular organs of adult mouse brains. *Glia*. 2013; 61(6):957–971. [PubMed: 23468425]
- Marinelli S, Di Marzo V, Berretta N, Matias I, Maccarrone M, Bernardi G, Mercuri NB. Presynaptic facilitation of glutamatergic synapses to dopaminergic neurons of the rat substantia nigra by endogenous stimulation of vanilloid receptors. *J Neurosci*. 2003; 23(8):3136–3144. [PubMed: 12716921]
- Marinelli S, Di Marzo V, Florenzano F, Fezza F, Viscomi MT, van der Stelt M, Bernardi G, Molinari M, Maccarrone M, Mercuri NB. N-arachidonoyl-dopamine tunes synaptic transmission onto

- dopaminergic neurons by activating both cannabinoid and vanilloid receptors. *Neuropsychopharmacology*. 2007; 32(2):298–308. [PubMed: 16760924]
- Martin E, Dahan D, Cardouat G, Gillibert-Duplantier J, Marthan R, Savineau JP, Ducret T. Involvement of TRPV1 and TRPV4 channels in migration of rat pulmonary arterial smooth muscle cells. *Pflugers Arch*. 2012; 464(3):261–272. [PubMed: 22820913]
- McIntyre P, McLatchie LM, Chambers A, Phillips E, Clarke M, Savidge J, Toms C, Peacock M, Shah K, Winter J, et al. Pharmacological differences between the human and rat vanilloid receptor 1 (VR1). *Br J Pharmacol*. 2001; 132(5):1084–1094. [PubMed: 11226139]
- Moreels M, Vandenabeele F, Dumont D, Robben J, Lambrechts I. Alpha-smooth muscle actin (alpha-SMA) and nestin expression in reactive astrocytes in multiple sclerosis lesions: potential regulatory role of transforming growth factor-beta 1 (TGF-beta1). *Neuropathol Appl Neurobiol*. 2008; 34(5):532–546. [PubMed: 18005096]
- Nishio T, Kawaguchi S, Yamamoto M, Iseda T, Kawasaki T, Hase T. Tenascin-C regulates proliferation and migration of cultured astrocytes in a scratch wound assay. *Neuroscience*. 2005; 132(1):87–102. [PubMed: 15780469]
- Pearce LV, Toth A, Ryu H, Kang DW, Choi HK, Jin MK, Lee J, Blumberg PM. Differential modulation of agonist and antagonist structure activity relations for rat TRPV1 by cyclosporin A and other protein phosphatase inhibitors. *Naunyn Schmiedebergs Arch Pharmacol*. 2008; 377(2):149–157. [PubMed: 18259730]
- Pekny M, Johansson CB, Eliasson C, Stakeberg J, Wallen A, Perlmann T, Lendahl U, Betsholtz C, Berthold CH, Frisen J. Abnormal reaction to central nervous system injury in mice lacking glial fibrillary acidic protein and vimentin. *J Cell Biol*. 1999; 145(3):503–514. [PubMed: 10225952]
- Phillips E, Reeve A, Bevan S, McIntyre P. Identification of species-specific determinants of the action of the antagonist capsaizine and the agonist PPAHV on TRPV1. *J Biol Chem*. 2004; 279(17):17165–17172. [PubMed: 14960593]
- Raisinghani M, Pabbidi RM, Premkumar LS. Activation of transient receptor potential vanilloid 1 (TRPV1) by resiniferatoxin. *J Physiol*. 2005; 567(Pt 3):771–786. [PubMed: 16037081]
- Renault-Mihara F, Okada S, Shibata S, Nakamura M, Toyama Y, Okano H. Spinal cord injury: emerging beneficial role of reactive astrocytes' migration. *Int J Biochem Cell Biol*. 2008; 40(9):1649–1653. [PubMed: 18434236]
- Ridley AJ, Schwartz MA, Burridge K, Firtel RA, Ginsberg MH, Borisy G, Parsons JT, Horwitz AR. Cell migration: integrating signals from front to back. *Science*. 2003; 302(5651):1704–1709. [PubMed: 14657486]
- Saadoun S, Papadopoulos MC, Watanabe H, Yan D, Manley GT, Verkman AS. Involvement of aquaporin-4 in astroglial cell migration and glial scar formation. *J Cell Sci*. 2005; 118(Pt 24):5691–5698. [PubMed: 16303850]
- Sakimoto S, Kidoya H, Naito H, Kamei M, Sakaguchi H, Goda N, Fukamizu A, Nishida K, Takakura N. A role for endothelial cells in promoting the maturation of astrocytes through the apelin/APJ system in mice. *Development*. 2012; 139(7):1327–1335. [PubMed: 22357924]
- Sappington RM, Calkins DJ. Contribution of TRPV1 to microglia-derived IL-6 and NFkappaB translocation with elevated hydrostatic pressure. *Invest Ophthalmol Vis Sci*. 2008; 49(7):3004–3017. [PubMed: 18362111]
- Sappington RM, Carlson BJ, Crish SD, Calkins DJ. The microbead occlusion model: a paradigm for induced ocular hypertension in rats and mice. *Invest Ophthalmol Vis Sci*. 2010; 51(1):207–216. [PubMed: 19850836]
- Sappington RM, Chan M, Calkins DJ. Interleukin-6 protects retinal ganglion cells from pressure-induced death. *Invest Ophthalmol Vis Sci*. 2006; 47(7):2932–2942. [PubMed: 16799036]
- Sappington RM, Sidorova T, Long DJ, Calkins DJ. TRPV1: contribution to retinal ganglion cell apoptosis and increased intracellular Ca<sup>2+</sup> with exposure to hydrostatic pressure. *Invest Ophthalmol Vis Sci*. 2009; 50(2):717–728. [PubMed: 18952924]
- Saunders CI, Kunde DA, Crawford A, Geraghty DP. Expression of transient receptor potential vanilloid 1 (TRPV1) and 2 (TRPV2) in human peripheral blood. *Mol Immunol*. 2007; 44(6):1429–1435. [PubMed: 16777226]

- Savidge J, Davis C, Shah K, Colley S, Phillips E, Ranasinghe S, Winter J, Kotsonis P, Rang H, McIntyre P. Cloning and functional characterization of the guinea pig vanilloid receptor 1. *Neuropharmacology*. 2002; 43(3):450–456. [PubMed: 12243775]
- Schneider CA, Rasband WS, Eliceiri KW. NIH Image to ImageJ: 25 years of image analysis. *Nat Methods*. 2012; 9(7):671–675. [PubMed: 22930834]
- Scott A, Powner MB, Gandhi P, Clarkin C, Gutmann DH, Johnson RS, Ferrara N, Fruttiger M. Astrocyte-derived vascular endothelial growth factor stabilizes vessels in the developing retinal vasculature. *PLoS One*. 2010; 5(7):e11863. [PubMed: 20686684]
- Seabrook GR, Sutton KG, Jarolimek W, Hollingworth GJ, Teague S, Webb J, Clark N, Boyce S, Kerby J, Ali Z, et al. Functional properties of the high-affinity TRPV1 (VR1) vanilloid receptor antagonist (4-hydroxy-5-iodo-3-methoxyphenylacetate ester) iodo-resiniferatoxin. *J Pharmacol Exp Ther*. 2002; 303(3):1052–1060. [PubMed: 12438527]
- Shao H, Travers T, Camacho CJ, Wells A. The carboxyl tail of alpha-actinin-4 regulates its susceptibility to m-calpain and thus functions in cell migration and spreading. *Int J Biochem Cell Biol*. 2013; 45(6):1051–1063. [PubMed: 23466492]
- Sofroniew MV. Molecular dissection of reactive astrogliosis and glial scar formation. *Trends Neurosci*. 2009; 32(12):638–647. [PubMed: 19782411]
- Song ZH, Zhong M. CB1 cannabinoid receptor-mediated cell migration. *J Pharmacol Exp Ther*. 2000; 294(1):204–209. [PubMed: 10871313]
- Sorci G, Agneletti AL, Bianchi R, Donato R. Association of S100B with intermediate filaments and microtubules in glial cells. *Biochim Biophys Acta*. 1998; 1448(2):277–289. [PubMed: 9920418]
- Suh YG, Oh U. Activation and activators of TRPV1 and their pharmaceutical implication. *Curr Pharm Des*. 2005; 11(21):2687–2698. [PubMed: 16101449]
- Sun D, Qu J, Jakobs TC. Reversible reactivity by optic nerve astrocytes. *Glia*. 2013; 61(8):1218–1235. [PubMed: 23650091]
- Szallasi A, Blumberg PM. Resiniferatoxin, a phorbol-related diterpene, acts as an ultrapotent analog of capsaicin, the irritant constituent in red pepper. *Neuroscience*. 1989; 30(2):515–520. [PubMed: 2747924]
- Tezel G, Hernandez MR, Wax MB. In vitro evaluation of reactive astrocyte migration, a component of tissue remodeling in glaucomatous optic nerve head. *Glia*. 2001; 34(3):178–189. [PubMed: 11329180]
- Toth A, Boczan J, Kedei N, Lizanecz E, Bagi Z, Papp Z, Edes I, Csiba L, Blumberg PM. Expression and distribution of vanilloid receptor 1 (TRPV1) in the adult rat brain. *Brain Res Mol Brain Res*. 2005a; 135(1–2):162–168. [PubMed: 15857679]
- Toth A, Wang Y, Kedei N, Tran R, Pearce LV, Kang SU, Jin MK, Choi HK, Lee J, Blumberg PM. Different vanilloid agonists cause different patterns of calcium response in CHO cells heterologously expressing rat TRPV1. *Life Sci*. 2005b; 76(25):2921–2932. [PubMed: 15820503]
- Wahl P, Foged C, Tullin S, Thomsen C. Iodo-resiniferatoxin, a new potent vanilloid receptor antagonist. *Mol Pharmacol*. 2001; 59(1):9–15. [PubMed: 11125018]
- Walpole CS, Bevan S, Bovermann G, Boelsterli JJ, Breckenridge R, Davies JW, Hughes GA, James I, Oberer L, Winter J, et al. The discovery of capsazepine, the first competitive antagonist of the sensory neuron excitants capsaicin and resiniferatoxin. *J Med Chem*. 1994; 37(13):1942–1954. [PubMed: 8027976]
- Walter L, Franklin A, Witting A, Moller T, Stella N. Astrocytes in culture produce anandamide and other acylethanolamides. *J Biol Chem*. 2002; 277(23):20869–20876. [PubMed: 11916961]
- Wang F, Smith NA, Xu Q, Fujita T, Baba A, Matsuda T, Takano T, Bekar L, Nedergaard M. Astrocytes modulate neural network activity by Ca<sup>2+</sup>-dependent uptake of extracellular K<sup>+</sup> Sci Signal. 2012; 5(218):ra26. [PubMed: 22472648]
- Wang JP, Tseng CS, Sun SP, Chen YS, Tsai CR, Hsu MF. Capsaicin stimulates the non-store-operated Ca<sup>2+</sup> entry but inhibits the store-operated Ca<sup>2+</sup> entry in neutrophils. *Toxicol Appl Pharmacol*. 2005; 209(2):134–144. [PubMed: 15882882]
- Waning J, Vriens J, Owsianik G, Stuwe L, Mally S, Fabian A, Frippiat C, Nilius B, Schwab A. A novel function of capsaicin-sensitive TRPV1 channels: involvement in cell migration. *Cell Calcium*. 2007; 42(1):17–25. [PubMed: 17184838]

- Watson MG, McDougall SR, Chaplain MA, Devlin AH, Mitchell CA. Dynamics of angiogenesis during murine retinal development: a coupled in vivo and in silico study. *J R Soc Interface*. 2012; 9(74):2351–2364. [PubMed: 22438490]
- Wei C, Wang X, Chen M, Ouyang K, Song LS, Cheng H. Calcium flickers steer cell migration. *Nature*. 2009; 457(7231):901–905. [PubMed: 19118385]
- Wei C, Wang X, Zheng M, Cheng H. Calcium gradients underlying cell migration. *Curr Opin Cell Biol*. 2012; 24(2):254–261. [PubMed: 22196933]
- Yang H, Wang Z, Capo-Aponte JE, Zhang F, Pan Z, Reinach PS. Epidermal growth factor receptor transactivation by the cannabinoid receptor (CB1) and transient receptor potential vanilloid 1 (TRPV1) induces differential responses in corneal epithelial cells. *Exp Eye Res*. 2010; 91(3):462–471. [PubMed: 20619260]
- Zhang Y, Porat RM, Alon T, Keshet E, Stone J. Tissue oxygen levels control astrocyte movement and differentiation in developing retina. *Brain Res Dev Brain Res*. 1999; 118(1–2):135–145.
- Zhao Z, Ni Y, Chen J, Zhong J, Yu H, Xu X, He H, Yan Z, Scholze A, Liu D, et al. Increased migration of monocytes in essential hypertension is associated with increased transient receptor potential channel canonical type 3 channels. *PLoS One*. 2012; 7(3):e32628. [PubMed: 22438881]
- Zhu D, Hu C, Sheng W, Tan KS, Haidekker MA, Sun AY, Sun GY, Lee JC. NAD(P)H oxidase-mediated reactive oxygen species production alters astrocyte membrane molecular order via phospholipase A2. *Biochem J*. 2009; 421(2):201–210. [PubMed: 19392662]
- Zimov S, Yazulla S. Localization of vanilloid receptor 1 (TRPV1/VR1)-like immunoreactivity in goldfish and zebrafish retinas: restriction to photoreceptor synaptic ribbons. *J Neurocytol*. 2004; 33(4):441–452. [PubMed: 15520529]
- Zygmunt PM, Petersson J, Andersson DA, Chuang H, Sorgard M, Di Marzo V, Julius D, Hogestatt ED. Vanilloid receptors on sensory nerves mediate the vasodilator action of anandamide. *Nature*. 1999; 400(6743):452–457. [PubMed: 10440374]

**Main Points**

Retinal astrocytes express the non-specific cation channel TRPV1. TRPV1 antagonism reduces migration in an *in vitro* scratch wound model by reducing calcium influx and modulating cytoskeletal filaments.

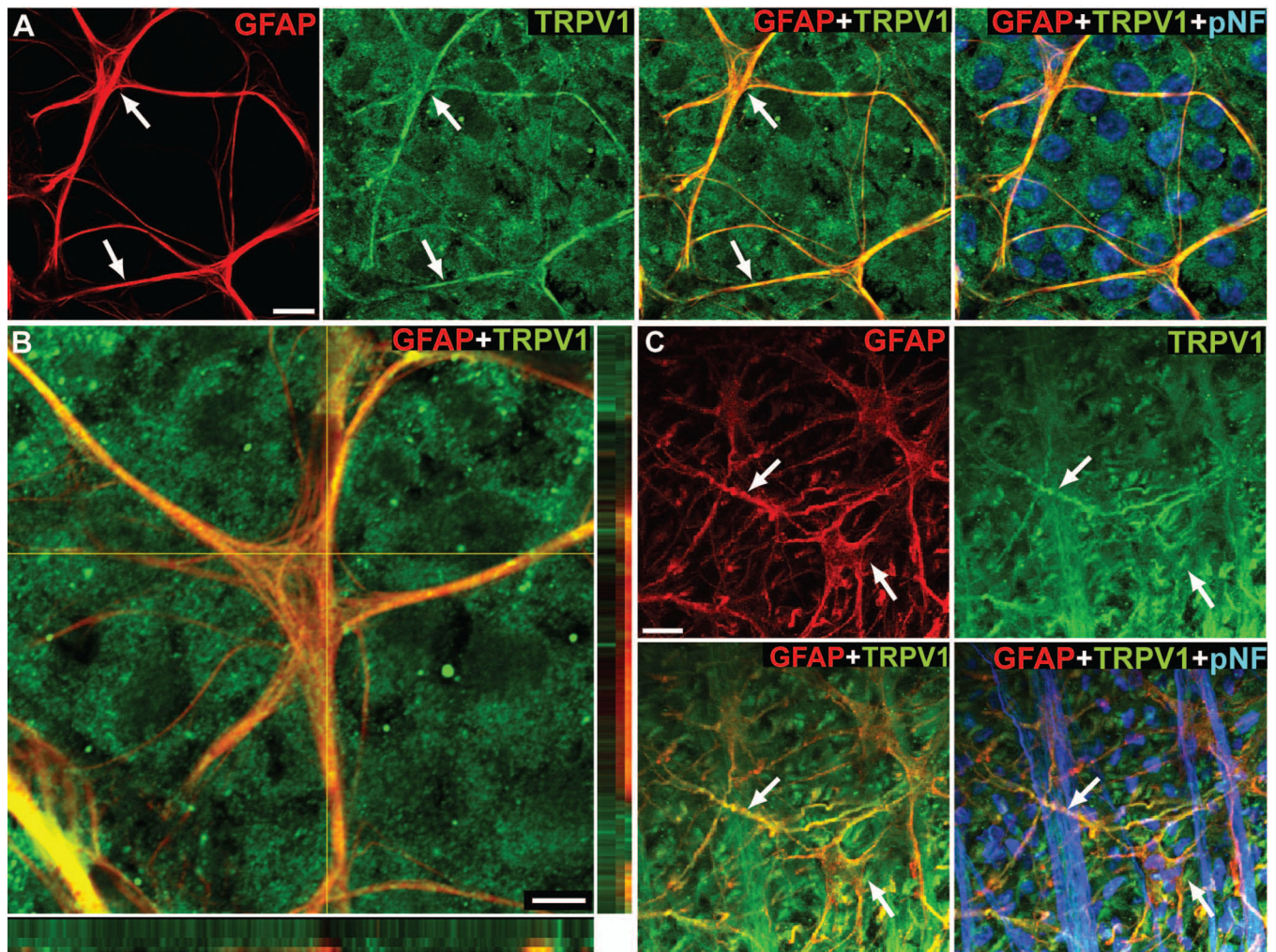


### Figure 1. Retinal astrocytes express TRPV1

Whole-mounted mouse (A, B) and rat (C) retinas demonstrate TRPV1 labeling (green) throughout processes and somas (arrows) of GFAP-positive astrocytes (red). Higher magnification and orthogonal views (B) show discrete colocalization of TRPV1 within GFAP-labeled astrocyte processes (yellow puncta). Scale: 10 μm (A and C); 5 μm (B).

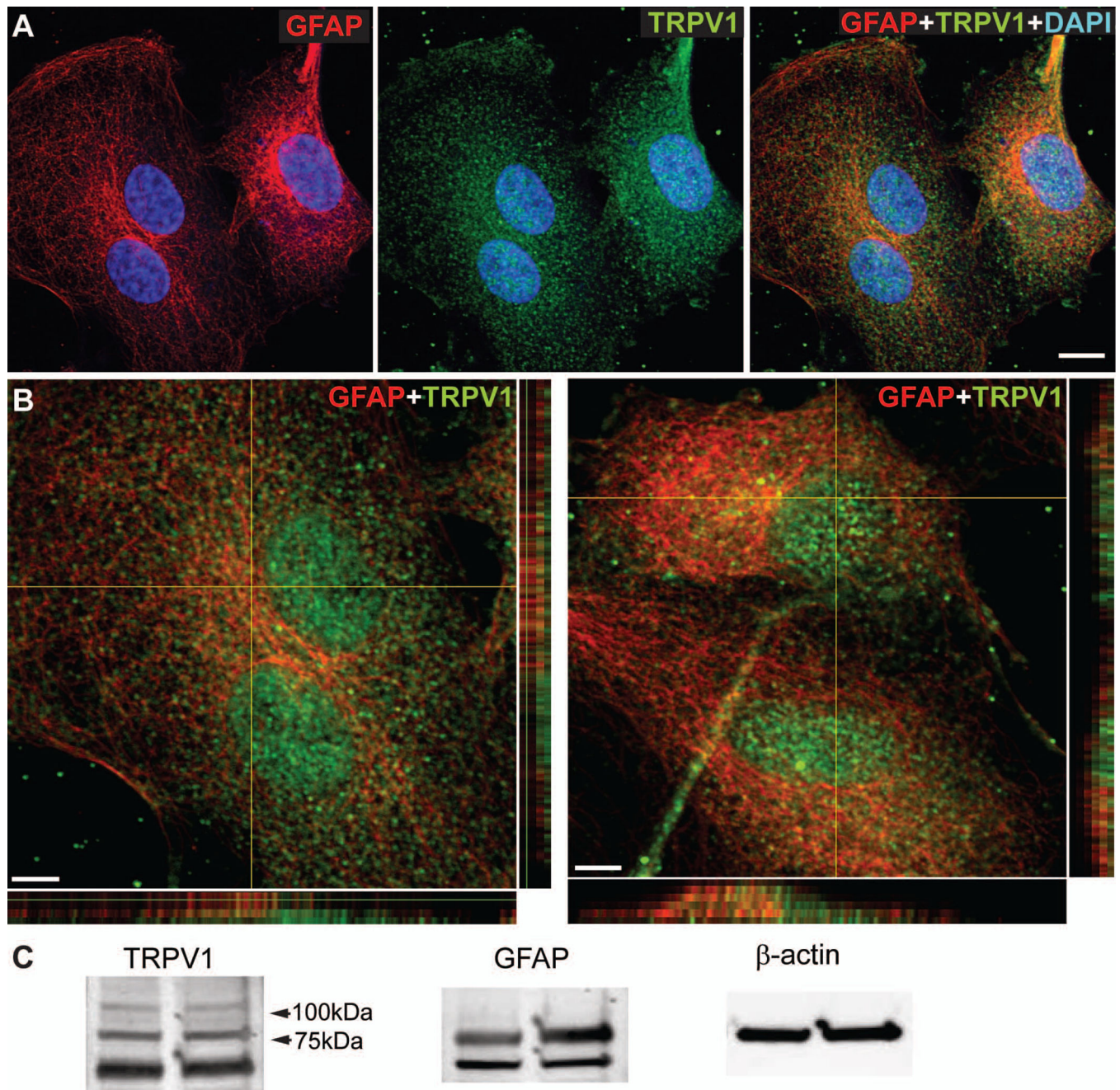


### Figure 2. Cultured retinal astrocytes express TRPV1

Cultures of primary retinal astrocytes (A) expressing GFAP (red) demonstrate diffuse TRPV1 labeling (green). Higher magnification and orthogonal views (B) demonstrate patches of TRPV1 (green) or GFAP (red) label as well as colocalization (yellow). Western blot analysis (C) shows expression of TRPV1 and GFAP in cultured astrocytes;  $\beta$ -actin is shown as loading control. Scale: 10  $\mu$ m (A); 5  $\mu$ m (B).

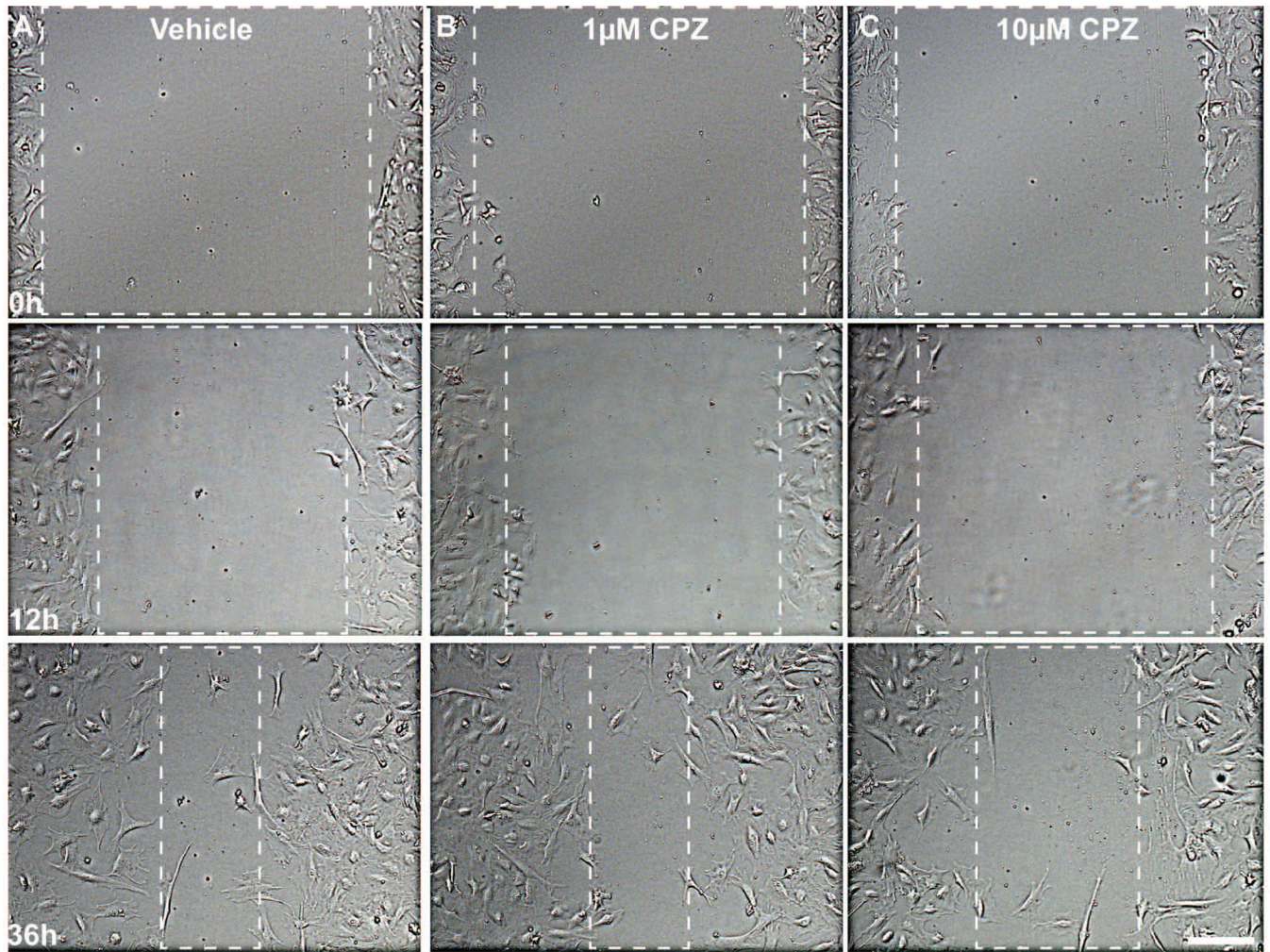


**Figure 3. Antagonism of TRPV1 reduces astrocyte migration**

Representative DIC images show astrocytes at 0, 12 and 36 h post-scratch for vehicle (A), 1 µM (B) and 10 µM (C) capsazepine (CPZ). Dashed boxes outline the wound area that was 95% cell-free. Scale: 200 µm.

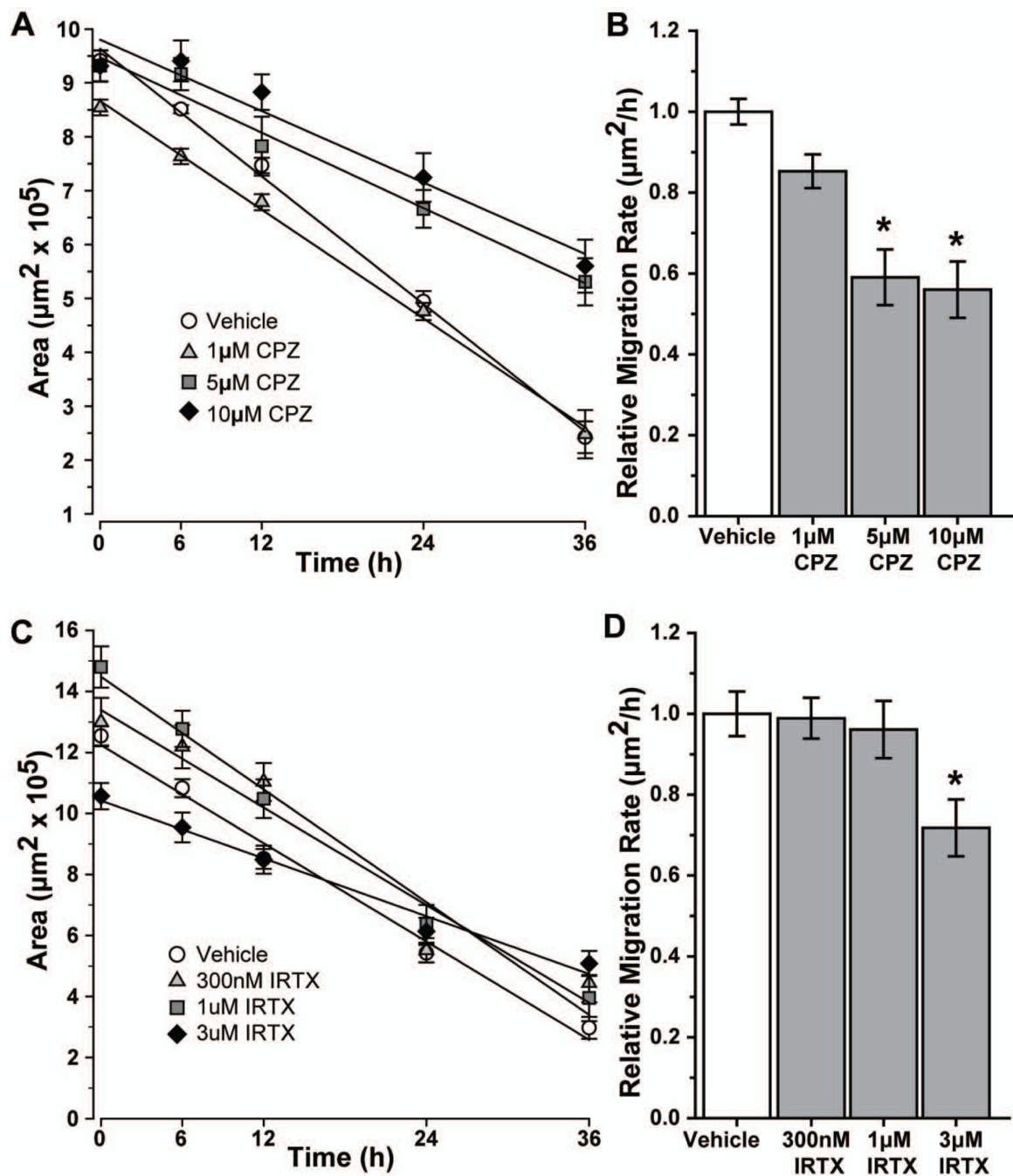


**Figure 4. Capsazepine and IRTX decrease rate of astrocyte migration**

Scatter plots show the change in average wound area over time for vehicle and various concentrations of capsazepine (CPZ; **A**) or 5'-iodo-resiniferatoxin (IRTX; **C**) treatments, along with the best-fitting regression line for each. Bar charts show migration rate relative to vehicle for CPZ (**B**) and IRTX (**D**). Significance compared to vehicle: \*,  $p = 0.006$  for CPZ; \*,  $p = 0.035$  for IRTX. All data: mean  $\pm$  SEM.

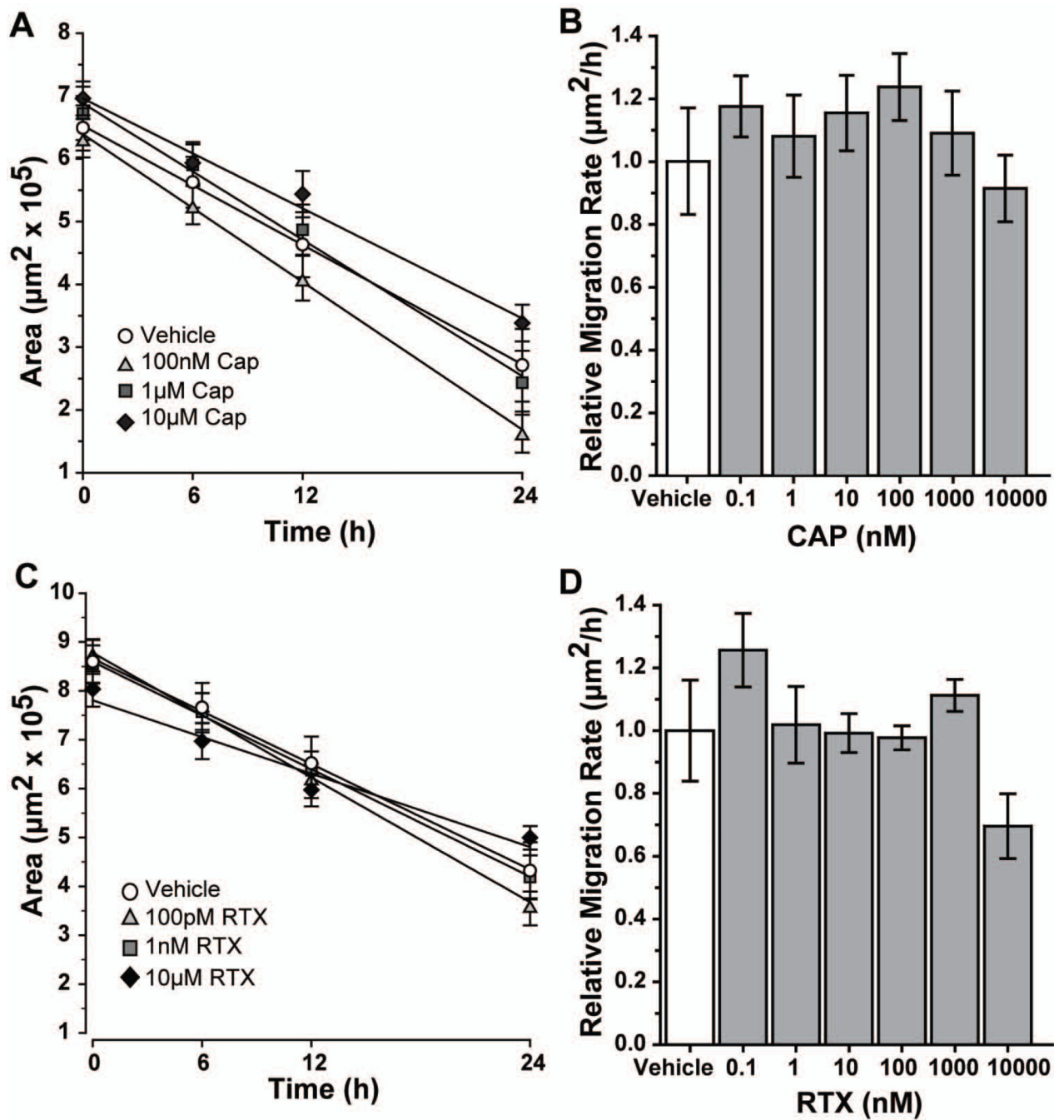


**Figure 5. Capsaicin and RTX have modest effects on astrocyte migration**

Scatter plots show the change in average wound area over time for vehicle and various concentrations of capsaicin (CAP; **A**) or resiniferatoxin (RTX; **C**) treatments, along with the best-fitting regression line for each. Bar charts show migration rate relative to vehicle for CAP (**B**) and RTX (**D**). All data: mean  $\pm$  SEM.

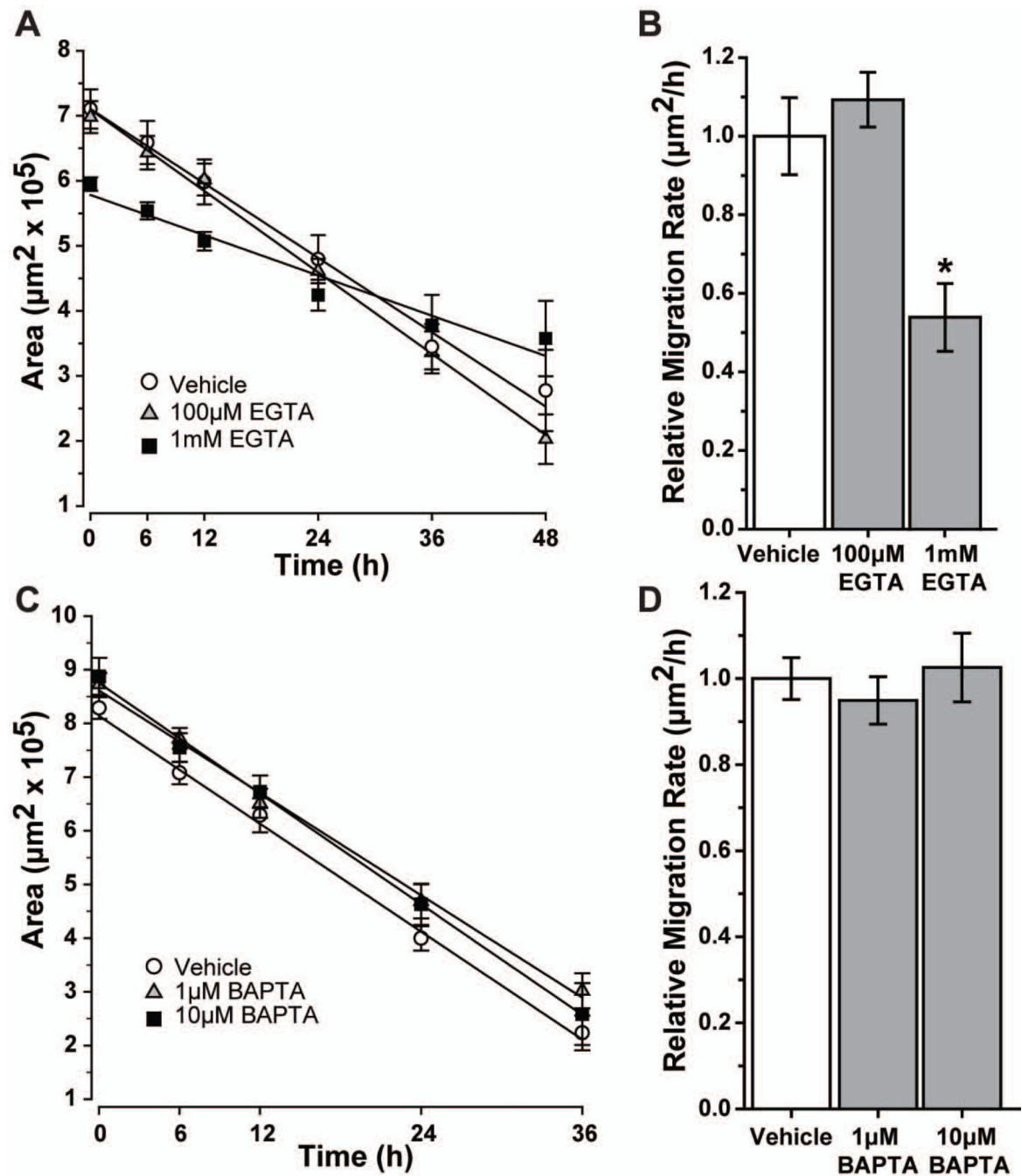


**Figure 6. Chelation of Ca<sup>2+</sup> with EGTA, but not BAPTA-AM reduces astrocyte migration**  
 Scatter plots show the change in average wound area over time for vehicle and various concentrations of EGTA (A) or BAPTA-AM (C), along with the best-fitting regression line for each. Migration rate relative to that for vehicle for EGTA (B) and BAPTA-AM (D) is graphed. Significance compared to vehicle: \*,  $p = 0.048$ . All data: mean  $\pm$  SEM.

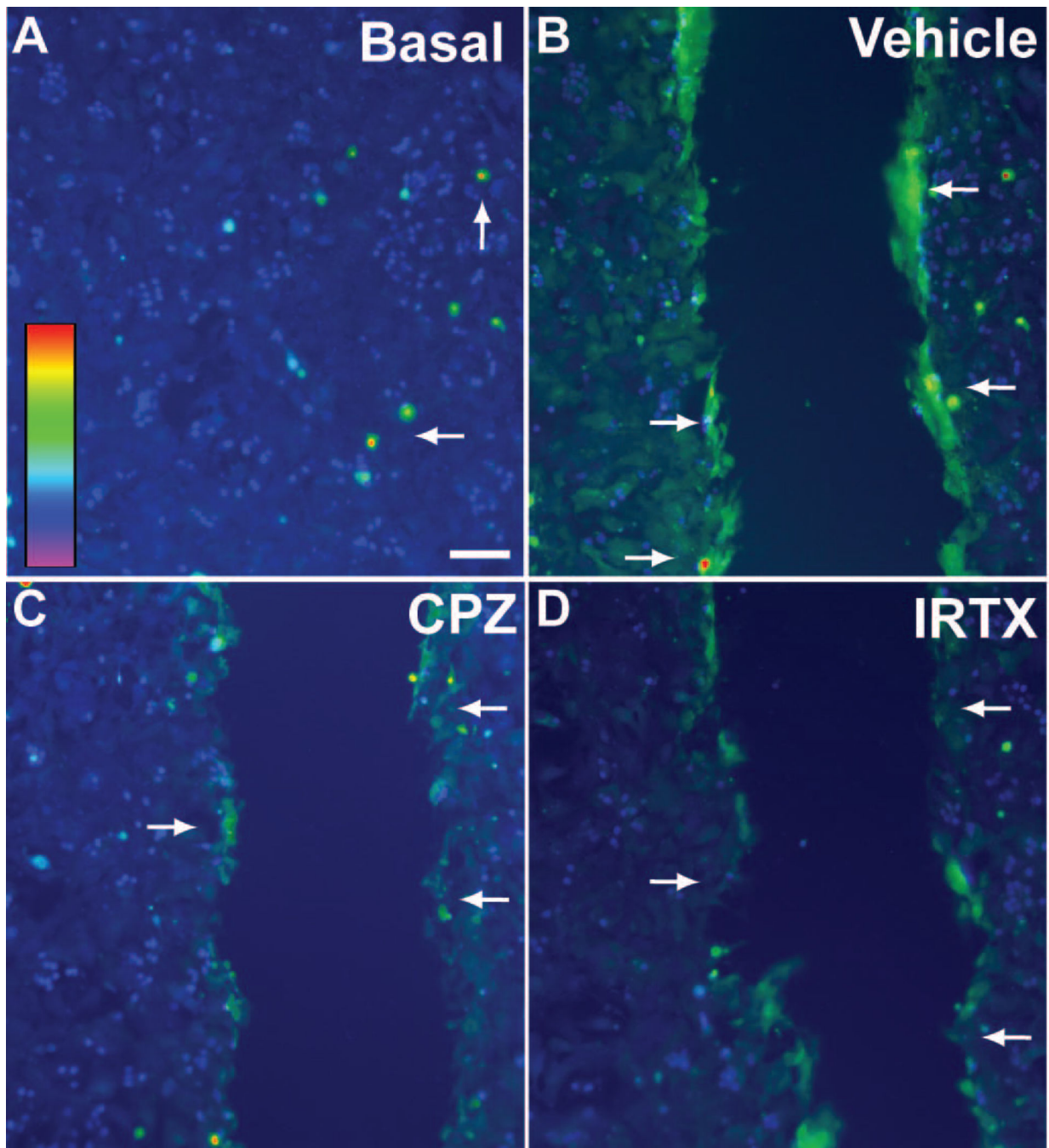


**Figure 7. Fura-2 AM imaging shows increased astrocyte intracellular Ca<sup>2+</sup> with injury**  
 Fluorescent image of astrocytes loaded with fura-2 AM shows modest basal intracellular levels in most cells. Arrows indicate cells with higher Ca<sup>2+</sup> levels. Inset shows scale of 340/380 nm ratio from low Ca<sup>2+</sup> levels (violet-blue) to high (orange-red) (A). Immediately following scratch wound (10 s), vehicle astrocytes (B) demonstrate increased intracellular Ca<sup>2+</sup> especially near the leading edge (arrows); 10 μM CPZ (C) and 3 μM IRTX (D) appear to reduce this increase. Scale: 100 μm.

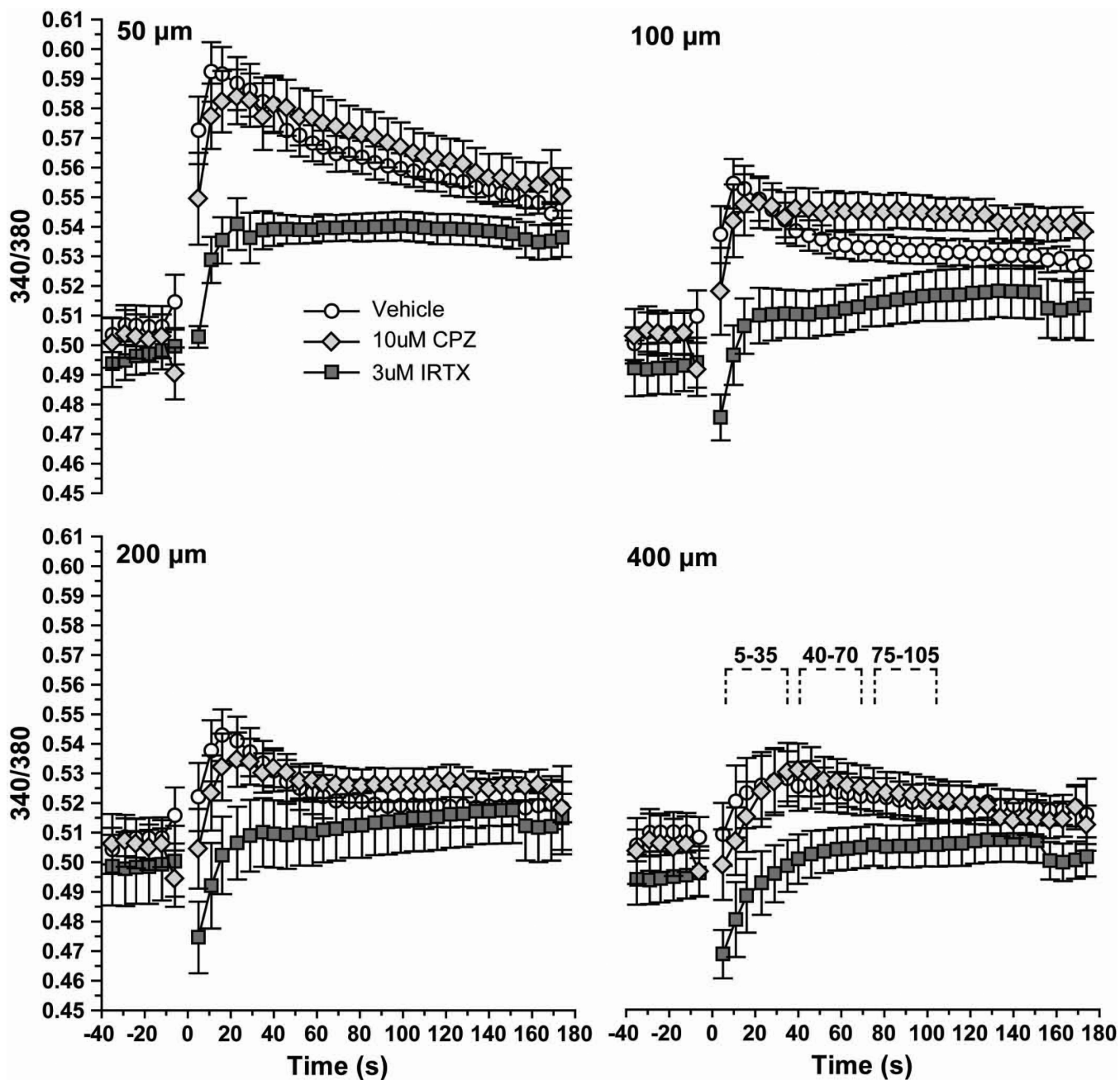


**Figure 8. Antagonism of TRPV1 reduces astrocyte intracellular  $Ca^{2+}$  following scratch injury**  
 Levels of astrocyte intracellular  $Ca^{2+}$  are expressed as the 340/380 nm fluorescence ratio before ( $< -5$  s) and following ( $> 5$  s) scratch injury ( $\sim 0$  s) for vehicle, 10  $\mu$ M CPZ and 3  $\mu$ M IRTX cells. Measurements were taken 50 to 400  $\mu$ m from the scratch leading edge. Inset for 400  $\mu$ m graph indicates post-injury time intervals quantified in Figure 9.

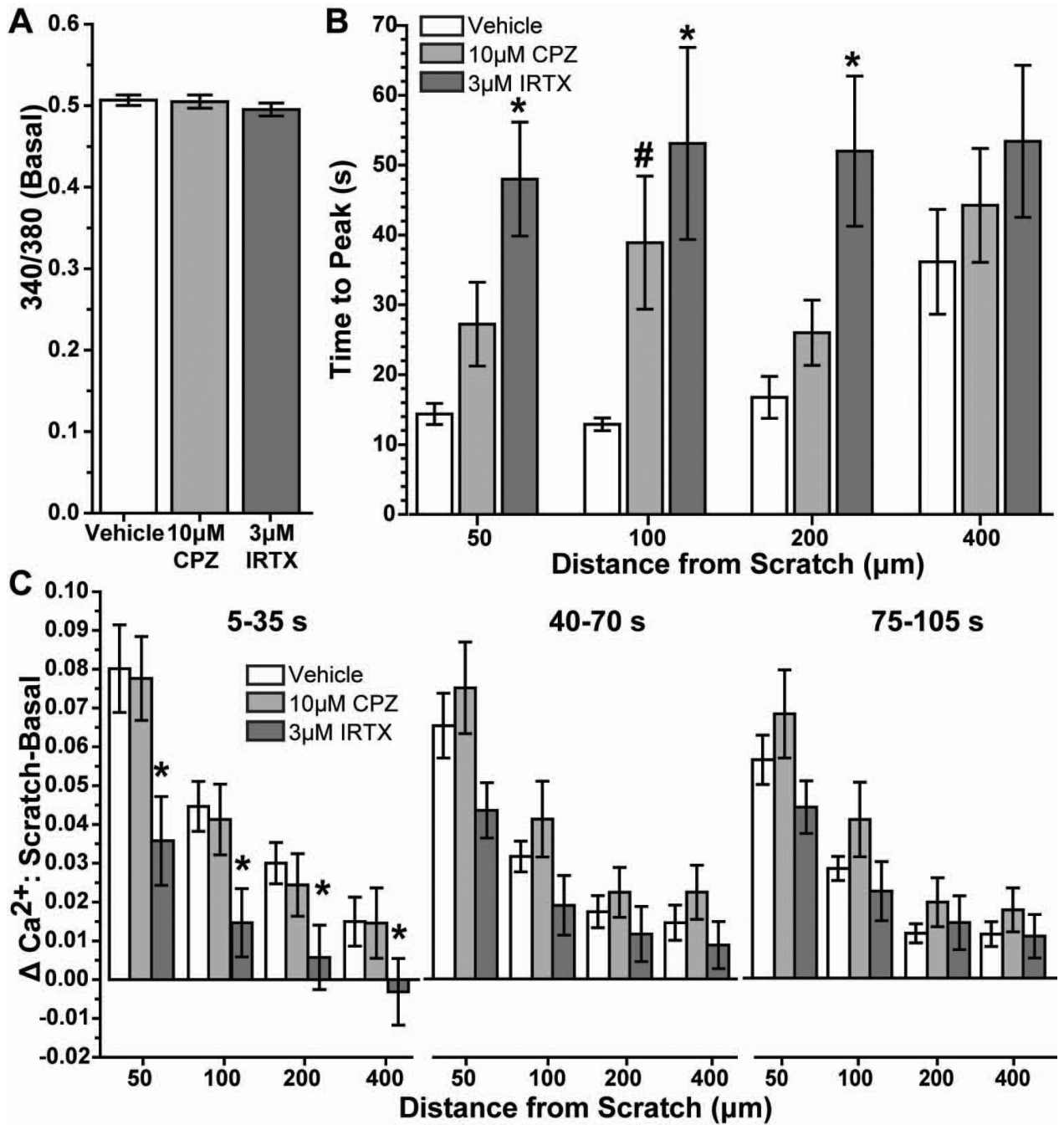


**Fig. 9. TRPV1 antagonism slows and reduces rise in astrocyte  $\text{Ca}^{2+}$  following injury**

Fura-2 AM 340/380 ratio prior to scratch wound shows astrocytes treated with vehicle, 10  $\mu$ M CPZ and 3  $\mu$ M IRTX have similar basal levels of intracellular  $\text{Ca}^{2+}$  (A). Bar chart shows time to reach peak 340/380  $\text{Ca}^{2+}$  ratio following scratch injury for each treatment at 50 to 400  $\mu$ m from the leading edge of the wound (B). Significance compared to vehicle: \*,  $p = 0.007$ ; #,  $p = 0.025$ . Bar chart shows the difference between scratch and basal 340/380  $\text{Ca}^{2+}$  ratio determined for various time intervals post-scratch at each distance from the injury (C). Significance compared to vehicle: \*,  $p = 0.04$ . All data: mean  $\pm$  SEM.

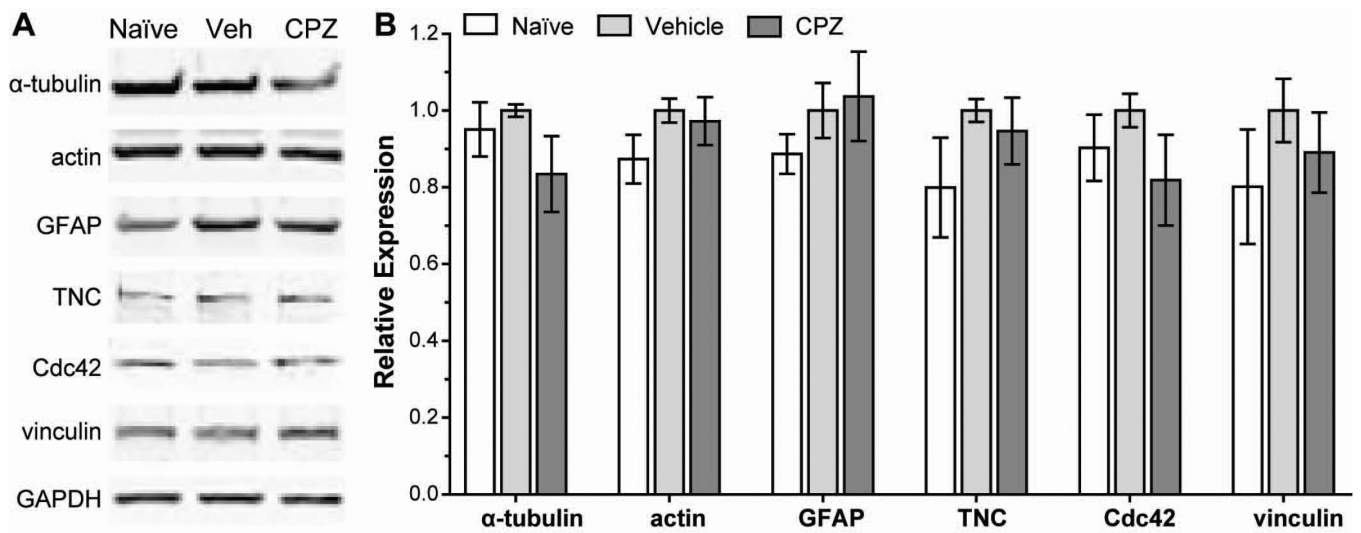


**Figure 10. Antagonism of TRPV1 reduces expression of cytoskeletal and migration-related proteins in astrocytes following scratch injury**

Western blots (**A**) and quantification (**B**) demonstrate expression of cytoskeletal proteins ( $\alpha$ -tubulin, actin and GFAP) and migration-related proteins (tenascin C, Cdc42 and vinculin) in cultured naïve astrocytes, and in astrocytes treated with vehicle or 5  $\mu$ M CPZ (CPZ) 12 h after scratch injury.

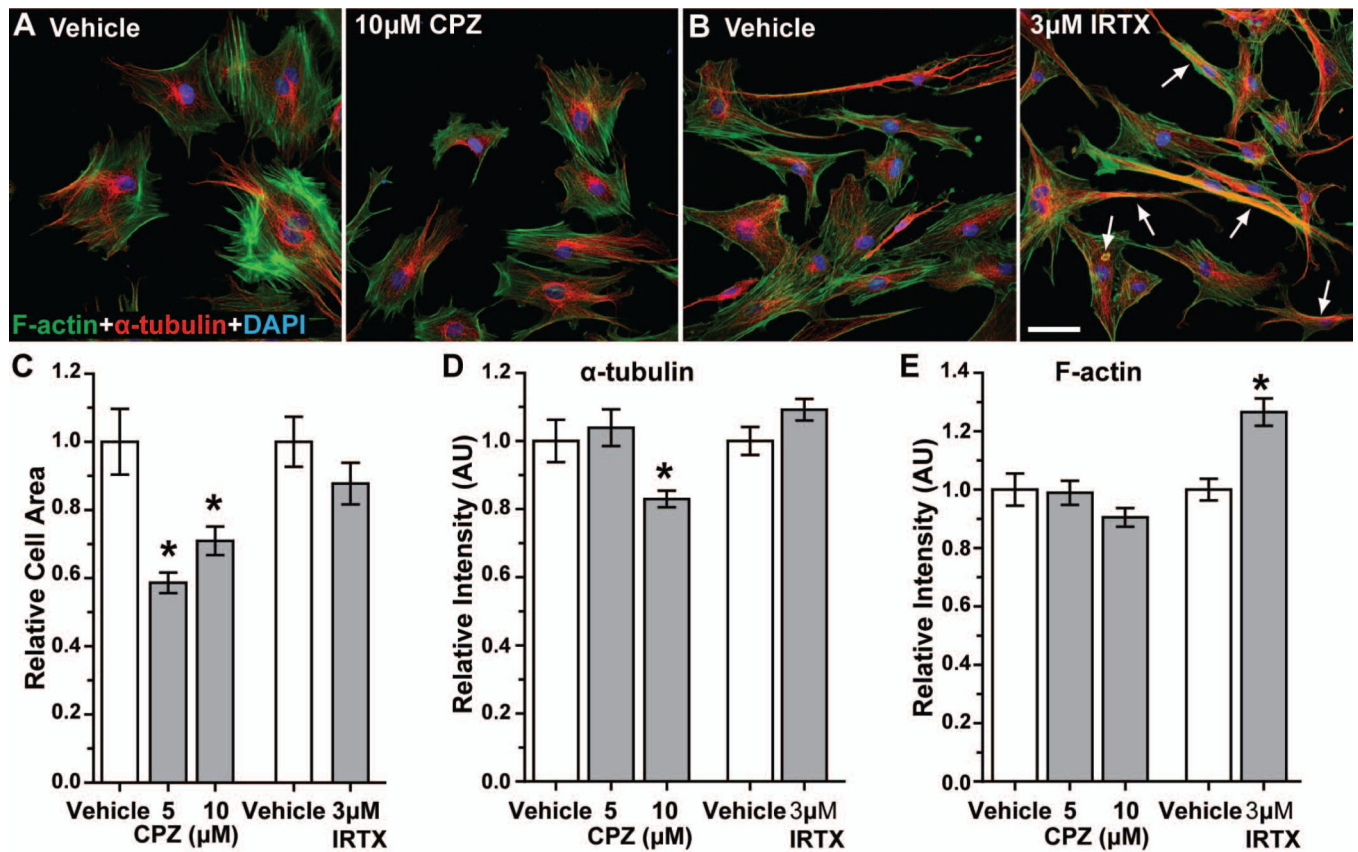


**Figure 11. Antagonism of TRPV1 reduces cell area and  $\alpha$ -tubulin intensity, while increasing F-actin intensity**

Confocal images show astrocytes near the leading edge 36 h following scratch wound labeled for F-actin (green),  $\alpha$ -tubulin (red) and DAPI (blue) for vehicle and 10  $\mu$ M CPZ treatments (A). Astrocytes treated with 3  $\mu$ M IRTX after scratch injury have increased colocalization of F-actin and  $\alpha$ -tubulin (arrows) (B). Scale: 50  $\mu$ m for A and B. Bar graph shows average astrocyte cytoplasmic area (C) normalized to vehicle for 5 and 10  $\mu$ M CPZ and 3  $\mu$ M IRTX treatments 36 hours post-migration. \*,  $p = 0.003$  compared to vehicle ( $n = 51$  cells). Bar graphs show the relative intensities of  $\alpha$ -tubulin (D) and F-actin (E) normalized to vehicle for CPZ and IRTX treatments. \*,  $p = 0.006$  compared to vehicle for  $\alpha$ -tubulin ( $n = 51$  cells); \*,  $p < 0.0001$  compared to vehicle for F-actin ( $n = 84$  cells). All data: mean  $\pm$  SEM.

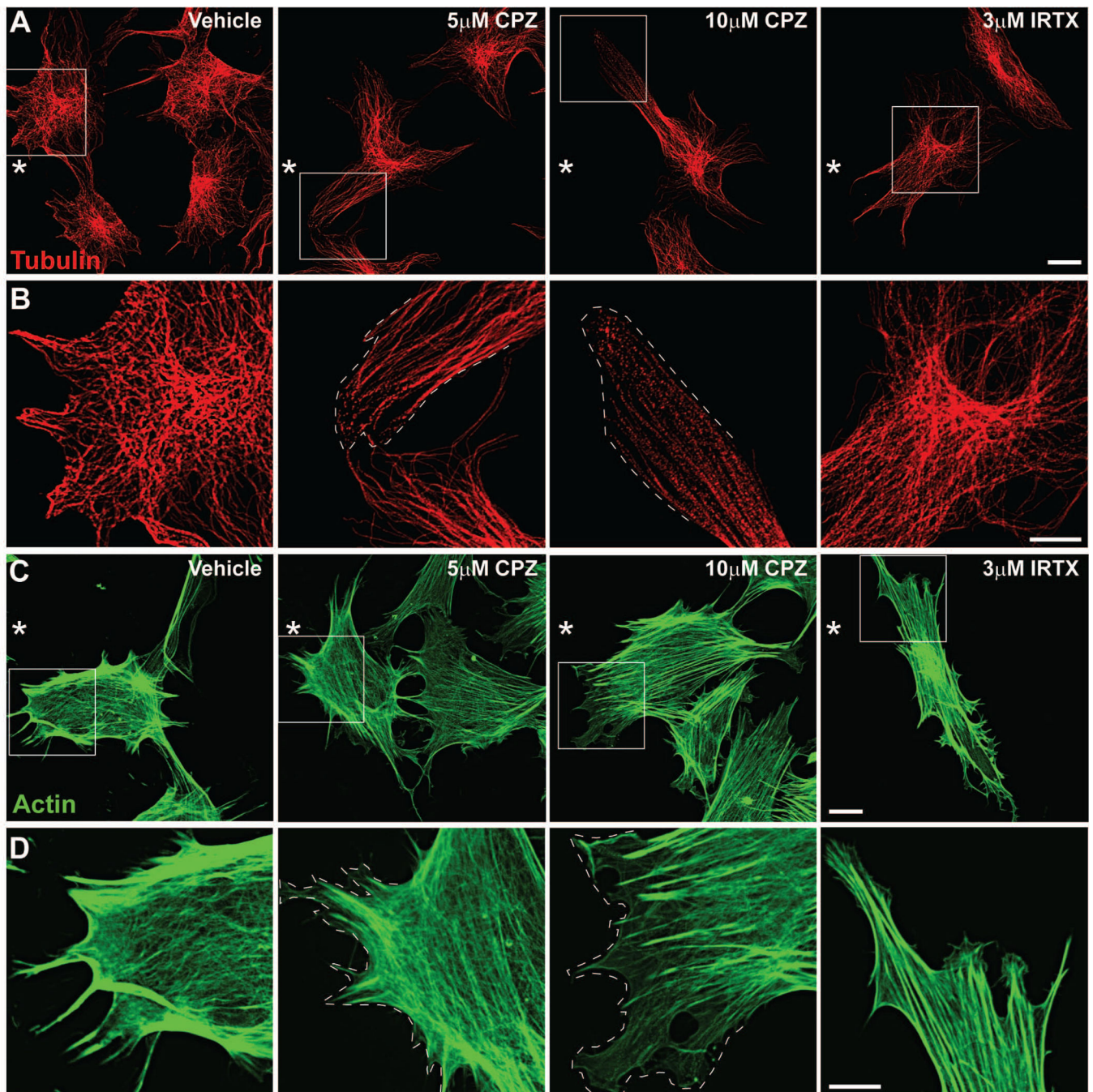


**Figure 12. Antagonism of TRPV1 alters  $\alpha$ -tubulin and actin subcellular localization**

High magnification (240 $\times$ ) confocal images show astrocytes near the leading edge of the wound (\*) 36 hours after scratch and labeled for  $\alpha$ -tubulin (red; **A**) and F-actin (green; **C**). High magnification views of boxed areas are shown in **B** and **D**. Cells were scratched in the presence of vehicle, 5  $\mu$ M or 10  $\mu$ M CPZ, or 3  $\mu$ M IRTX and then fixed in an extraction buffer for cytoskeletal proteins prior to labeling. Dotted lines represent cell edge. Scale: 20  $\mu$ m (**A** and **C**) and 10  $\mu$ m (**B** and **D**).

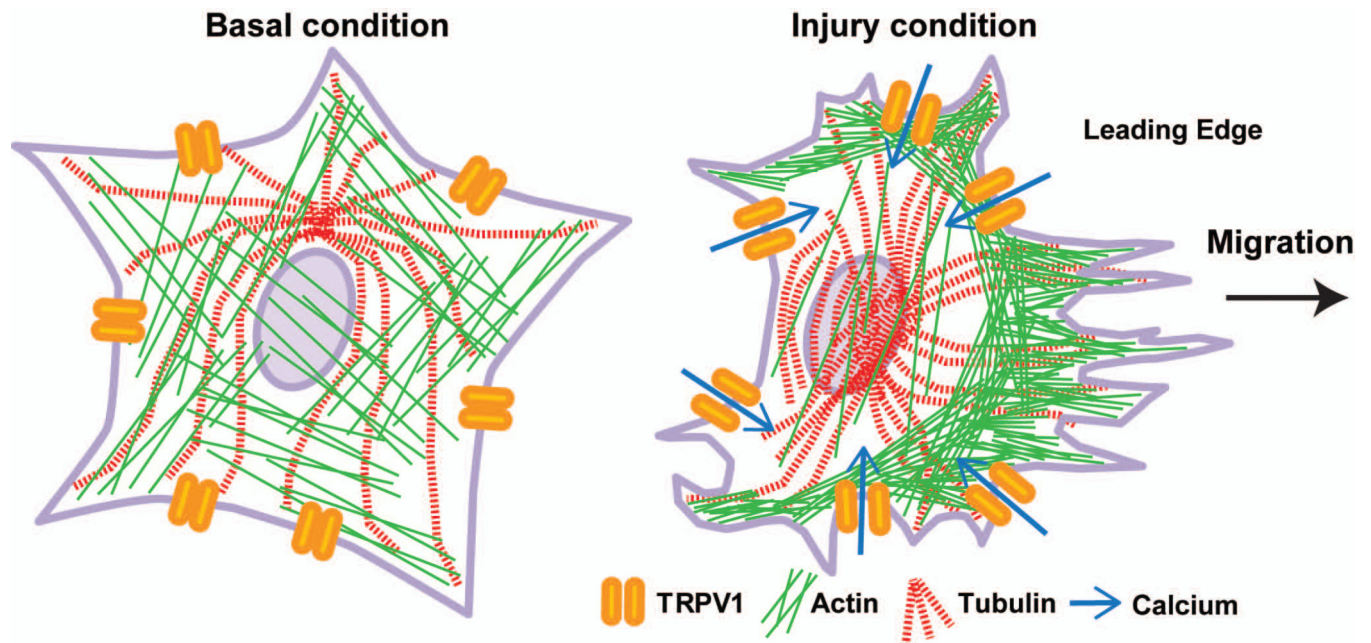


**Figure 13. TRPV1 contributes to retinal astrocyte migration following injury through cytoskeletal rearrangement via a  $\text{Ca}^{2+}$  dependent mechanism**

Schematic shows microtubules and actin fibers in retinal astrocytes under basal conditions and after injury. Based on our data, we hypothesize that following injury TRPV1 expressed by retinal astrocytes becomes activated and  $\text{Ca}^{2+}$  enters the cell. Microtubules undergo rearrangement to establish cell polarity and actin filaments localize to filopodia at the leading edge. This rearrangement of cytoskeletal proteins results in astrocyte migration toward the injury site.